The Astrophysical Journal, 671:497–517, 2007 December 10

AMBIPOLAR DIFFUSION IN MOLECULAR CLOUD CORES AND THE GRAVOMAGNETO CATASTROPHE

Fred C. Adams[1,2] and Frank H. Shu[3]
Received 2007 July 16; accepted 2007 August 30

ABSTRACT

This paper reexamines the problem of ambipolar diffusion as a mechanism for the production and runaway evolution of centrally condensed molecular cloud cores, a process that has been termed the gravomagneto catastrophe. Our calculation applies in the geometric limit of a highly flattened core and allows for a semianalytic treatment of the full problem, although physical fixes are required to resolve a poor representation of the central region. A noteworthy feature of the overall formulation is that the solutions for the ambipolar diffusion portion of the evolution for negative times ($t < 0$) match smoothly onto the collapse solutions for positive times ($t > 0$). The treatment shows that the resulting cores display nonzero, but submagnetosonic, inward velocities at the end of the diffusion epoch, in agreement with current observations. Another important result is the derivation of an analytic relationship between the dimensionless mass-to-flux ratio $\lambda_0 \equiv f_0^{-1}$ of the central regions produced by runaway core condensation and the dimensionless measure of the rate of ambipolar diffusion ϵ. In conjunction with previous work showing that ambipolar diffusion takes place more quickly in the presence of turbulent fluctuations, i.e., that the effective value of ϵ can be enhanced by turbulence, the resultant theory provides a viable working hypothesis for the formation of isolated molecular cloud cores and their subsequent collapse to form stars and planetary systems.

Subject headings: methods: analytical — MHD — stars: formation

1. INTRODUCTION

Since molecular clouds are supported, at least in part, by magnetic fields, the removal of magnetic fields represents an important component of the star formation process. In the most studied scenario, field removal occurs through the action of ambipolar diffusion, wherein magnetic fields are tied to the ionized component, which drifts relative to the more dominant neutral component of the gas (Mestel & Spitzer 1956; Mouschovias 1976; Nakano 1979, 1984; Shu 1983; Lizano & Shu 1989; Basu & Mouschovias 1994). The neutral gas thus condenses inward toward a quasi-hydrostatic state, although perfect equilibrium is generally not reached. When the condensing gas becomes sufficiently centrally concentrated, the innermost regions of the structure begin to collapse dynamically onto a growing pointlike protostar and eventually approach ballistic (free-fall) conditions.

Because of its large dynamic range in space and time, the process is not easy to follow numerically. The magnetic field and the forces that it exerts are vector quantities, so the relevant diffusion and dynamic equations are generally nonlinear, coupled partial differential equations in multiple spatial dimensions. The assumption of axial symmetry provides some simplification, but one still needs to deal with two spatial dimensions and time. In spite of these complications, the net result is physically simple. As magnetic fields diffuse outward, gas condenses inward to form a centrally concentrated structure that approaches pure power-law distributions of gas density, magnetic field, and other quantities (Nakano 1979; Lizano & Shu 1989; Basu & Mouschovias 1994). The goal of this paper is to demonstrate in a simple mathematical fashion how the asymptotic state is reached through nearly self-similar evolution toward a gravomagneto catastrophe, wherein an infinite central concentration is formally reached in finite time. After this point of catastrophe, set equal to the pivotal time $t = 0$, the system experiences true dynamical collapse to form a pointlike star, which will be surrounded by a centrifugally supported disk due to the precollapse rotation of the cloud core. Note that this study does not include the effects of rotation, so that the collapse solutions found herein represent the outer portion of the collapse flow; these solutions can then be matched onto inner solutions that include rotation and other effects (e.g., Cassen & Moosman 1981; Terebey et al. 1984; Jijina & Adams 1996).

Although molecular cloud cores experiencing ambipolar diffusion were identified as playing a dominant role in the formation of isolated low-mass stars two decades ago (Shu et al. 1987), recent observations indicate that ambipolar diffusion takes place more rapidly than the simple laminar description (e.g., Jijina et al. 1999). In addition, nonzero inflow velocities are often observed in starless cores (Lee et al. 2001; Harvey et al. 2002), which are assumed to be precollapse states. Contrary to popular perception, both of these properties can be accommodated within the picture of core formation via ambipolar diffusion. Indeed, one of the principal results of this paper is to calculate the nonzero, but submagnetosonic, inward velocity resulting from the ambipolar diffusion process. Despite this faster evolution, molecular cloud cores are well-defined entities and not transient, turbulent phenomena (Lada et al. 2008). As a consequence of their linkage to strong magnetic fields, probably, these cores are also restrained from moving ballistically through their parent clouds (Walsh et al. 2004).

The rest of this paper is organized as follows. We present the formulation of the problem in terms of physical variables in § 2, where we enforce axial symmetry and use a flattened approximation. The following section (§ 3) outlines our approach to solving the resulting problem. We first apply a similarity transformation, which converts the partial integro-differential equations into ordinary integro-differential equations. Since the diffusion timescale is comparable to or longer than the magnetosonic timescale needed to cross from the core center to the boundary where the core attaches to a common envelope, the solution to the induction equation itself requires a more complicated approach. In § 4 we solve the zeroth-order condensation problem for $t < 0$ to describe the approach to the pivotal instant $t = 0$ of gravomagneto catastrophe.

[1] Michigan Center for Theoretical Physics, Physics Department, University of Michigan, Ann Arbor, MI 48109.
[2] Astronomy Department, University of Michigan, Ann Arbor, MI 48109.
[3] Center for Astrophysics and Space Sciences, Physics Department, University of California, La Jolla, CA 92093.

As a simplification, we use the monopole (split monopole) approximation for the gravitational (magnetic tension) forces, thereby transforming the integro-differential equations to ordinary differential equations that are solved by standard methods. In § 5 we point out the shortcomings at large and small radii of the monopole approximation, and we generalize the approach by adopting various mathematical and physical fixes that show how the general physical problem possesses condensation solutions that connect smoothly to marginally critical envelopes. A central result of this section is the analytic derivation of a relationship between the dimensionless rate of ambipolar diffusion ϵ and the dimensionless flux-to-mass ratio $f_0 \equiv \lambda_0^{-1}$ of the central regions of the condensing core at the moment of gravomagneto catastrophe. In § 6 we demonstrate how the runaway condensation that characterizes gravomagneto catastrophe transitions smoothly for $t > 0$ to dynamically collapsing states that correspond to cores with accreting pointlike protostars, i.e., the infall-collapse solutions that have been used widely in previous studies of star formation. In § 7 we present a specific dimensional example to illustrate the typical astronomical characteristics of the entire process on both sides of the pivotal instant $t = 0$. We conclude in § 8 with a summary of the astronomical implications of our results. Finally, in a series of Appendices A–F we develop and extend various technical points encountered in the discussion of the text.

2. FORMULATION

The basic evolutionary equations for a flattened, self-gravitating cloud core of surface density Σ and radial velocity u, threaded by a magnetic field with vertical component B_z, are taken from the analysis of Shu & Li (1997) to be as follows. The equation of continuity is given by

$$\frac{\partial \Sigma}{\partial t} + \frac{1}{\varpi}\frac{\partial}{\partial \varpi}(\varpi u \Sigma) = 0. \tag{1}$$

The force equation is

$$\frac{\partial u}{\partial t} + u\frac{\partial u}{\partial \varpi} + \frac{a^2}{\Sigma}\frac{\partial}{\partial \varpi}(\Theta\Sigma) = g + \ell, \tag{2}$$

where the acceleration produced by self-gravitation plus magnetic tension, $g + \ell$, is given by

$$g + \ell = \frac{1}{\varpi^2 \Sigma}\int_0^\infty K_0\left(\frac{r}{\varpi}\right)\left[-G\Sigma(\varpi)\Sigma(r) + \frac{B_z(\varpi)B_z(r)}{(2\pi)^2}\right]2\pi r\, dr, \tag{3}$$

and the kernel K_0 is defined via

$$K_0(q) = \frac{1}{2\pi}\int_0^{2\pi}\frac{(1 - q\cos\varphi)d\varphi}{(1 + q^2 - 2q\cos\varphi)^{3/2}}. \tag{4}$$

In equation (2), a is the gaseous isothermal sound speed, and Θ provides the correction for the effects of the magnetic pressure (see Appendix A). Finally, the induction equation, which governs the evolution of the vertical component of the magnetic field threading the core in the presence of ambipolar diffusion, takes the form (see Appendix B)

$$\Sigma\left[\frac{\partial B_z}{\partial t} + \frac{1}{\varpi}\frac{\partial}{\partial \varpi}(\varpi u B_z)\right] = \frac{1}{\varpi}\frac{\partial}{\partial \varpi}\left[\frac{(2z_0)^{1/2}}{2\pi\gamma\mathcal{C}}\frac{\varpi B_z^2 B_\varpi^+}{\Sigma^{1/2}}\right], \tag{5}$$

where we have defined the radial component of the field at the upper vertical surface of the core by

$$B_\varpi^+ = \frac{1}{\varpi^2}\int_0^\infty K_0\left(\frac{r}{\varpi}\right)B_z(r)r\, dr. \tag{6}$$

The half-height z_0 appearing in equation (5) is defined by the assumed vertical hydrostatic equilibrium (Appendix A). The quantities γ and $1/\mathcal{C}$ are, respectively, the usual drag coefficient between ions and neutrals and the height-averaged reciprocal coefficient for the ion mass abundance (see Appendix B and chapter 27 of Shu 1992). An attractive feature of the approach presented in this paper is that we can delay specifying the actual numerical value of the product $\gamma\mathcal{C}$ until it comes to specifying dimensional scalings appropriate to specific astronomical objects, as long as the combination of parameters given by equation (20) below is a small number compared to unity.

We define the dimensionless ratio λ of mass per unit area to flux per unit area according to

$$\lambda = \frac{2\pi G^{1/2}\Sigma}{B_z}. \tag{7}$$

Appendix A derives expressions for Θ and z_0 in terms of λ for a magnetized singular isothermal disk, the form that our inner core approaches asymptotically at the moment of gravomagneto catastrophe. These relationships have the elegance of simplicity, and we adopt the approximation that the following expressions from Appendix A hold for all time, i.e.,

$$\Theta = \frac{2 + \lambda^2}{1 + \lambda^2}, \quad z_0 = \left(\frac{\lambda^2}{1 + \lambda^2}\right)\frac{a^2}{\pi G\Sigma}. \tag{8}$$

Combined with equations (1), (2), and (5), the relationships from equations (7) and (8) give us a closed set of equations to solve for Σ, u, B_z, λ, Θ, and z_0.

3. HOMOLOGY, SELF-SIMILARITY, AND ASYMPTOTICS

In this section we construct a similarity transformation to recast the problem in simpler form. First, we want to simplify the magnetic induction equation by using equation (7) and by making the (usual) approximation that the combination $\gamma\mathcal{C}$ is a constant during the phase of molecular cloud core formation. As a result, equation (5) takes the form

$$\Sigma^2\left(\frac{\partial}{\partial t} + u\frac{\partial}{\partial \varpi}\right)\frac{1}{\lambda} = \sqrt{\frac{2}{\pi}}\left(\frac{a}{\gamma\mathcal{C}}\right)\frac{1}{\varpi}\frac{\partial}{\partial \varpi}\left[\frac{\varpi\Sigma B_\varpi^+}{\lambda(1 + \lambda^2)^{1/2}}\right], \tag{9}$$

With this transformation, the definition of B_ϖ^+ becomes

$$B_\varpi^+ = \frac{2\pi G^{1/2}}{\varpi^2}\int_0^\infty r\, dr\, K_0\left(\frac{r}{\varpi}\right)\frac{\Sigma(r)}{\lambda(r)}. \tag{10}$$

Similarly, the force terms now have the form

$$g + \ell = \frac{2\pi G}{\varpi^2}\int_0^\infty K_0\left(\frac{r}{\varpi}\right)\Sigma(r)r\, dr\left[-1 + \frac{1}{\lambda(r)\lambda(\varpi)}\right]. \tag{11}$$

3.1. *Basic Similarity Transformation*

With the form of the magnetic induction equation specified, we now transform from a (ϖ, t) description to a (x, t) description, where we use the relations

$$x = \frac{\varpi}{a|t|}, \quad \Sigma(\varpi, t) = \frac{a}{2\pi G|t|}\tilde{\sigma}(x, t),$$
$$u(\varpi, t) = a\tilde{v}(x, t), \quad B_z(\varpi, t) = \frac{a}{G^{1/2}|t|}\tilde{\beta}(x, t). \tag{12}$$

In the simplest type of transformation, self-similarity of the first kind (Barenblatt 1996), the functions $\tilde{\sigma}$, $\tilde{v}$, and $\tilde{\beta}$ introduced here would be functions of the similarity variable x only. In this case, however, we allow the functions to retain an additional time dependence to account for the fact that ambipolar diffusion occurs on a longer timescale than the runaway dynamics. Note also that we have written the time variable in the coefficients with absolute value signs. We wish to mark the pivotal time $t = 0$ as the moment of gravomagneto catastrophe, so that positive times correspond to the self-similar solutions of gravitational collapse onto a pointlike protostar (Li & Shu 1997), whereas negative times correspond to the epoch of ambipolar diffusion in starless cores. The start of the ambipolar diffusion process thus corresponds to the limit $t \to -\infty$, and the end of the ambipolar diffusion epoch corresponds to the limit $t \to 0^-$.

With this choice of transformation, the dimensionless mass-to-flux ratio is given by

$$\lambda = \lambda(x, t) = \frac{\tilde{\sigma}(x, t)}{\tilde{\beta}(x, t)}. \tag{13}$$

We also define its inverse, i.e., the dimensionless flux-to-mass ratio,

$$f(x, t) \equiv \frac{1}{\lambda(x, t)} = \frac{\tilde{\beta}(x, t)}{\tilde{\sigma}(x, t)}. \tag{14}$$

The derivatives then take the forms

$$\left(\frac{\partial}{\partial t}\right)_{\varpi} = \left(\frac{\partial}{\partial t}\right)_{x} + \frac{x}{|t|}\frac{\partial}{\partial x}, \tag{15}$$

$$\left(\frac{\partial}{\partial \varpi}\right)_{t} = \frac{1}{a|t|}\frac{\partial}{\partial x}. \tag{16}$$

With this formulation, the equation of continuity is given by

$$|t|\frac{\partial \tilde{\sigma}}{\partial t} + \left(1 + x\frac{\partial}{\partial x}\right)\tilde{\sigma} + \frac{1}{x}\frac{\partial}{\partial x}(x\tilde{v}\tilde{\sigma}) = 0. \tag{17}$$

The force equation then becomes

$$|t|\frac{\partial \tilde{v}}{\partial t} + (x + \tilde{v})\frac{\partial \tilde{v}}{\partial x} + \frac{1}{\tilde{\sigma}}\frac{\partial}{\partial x}(\Theta\tilde{\sigma})$$
$$= \int_0^\infty K_0\left(\frac{y}{x}\right)\tilde{\sigma}(y, t)[\, f(x, t)f(y, t) - 1]\frac{y\, dy}{x^2}. \tag{18}$$

The induction equation can be written

$$\tilde{\sigma}^2\left[|t|\frac{\partial f}{\partial t} + (x + \tilde{v})\frac{\partial f}{\partial x}\right] = \frac{\epsilon}{x}\frac{\partial}{\partial x}\left[x\tilde{\sigma}\tilde{b}\left(\frac{f^2}{\sqrt{1 + f^2}}\right)\right], \tag{19}$$

where we have defined

$$\epsilon \equiv \frac{\sqrt{8\pi G}}{\gamma\mathcal{C}}, \tag{20}$$

so that ϵ is a small dimensionless parameter of the problem (essentially the ratio of dynamical time to the diffusion time; see also Galli & Shu 1993, who denoted a similar inverse ratio as a large parameter χ). In addition, the reduced radial magnetic field $\tilde{b}$ is defined in terms of the integral

$$\tilde{b}(x, t) = \frac{1}{x^2}\int_0^\infty K_0\left(\frac{y}{x}\right)\tilde{\sigma}(y, t)f(y, t)y\, dy. \tag{21}$$

If we use the traditional microscopic values of $\gamma = 3.5 \times 10^{13}$ cm^3 g^{-1} s^{-1} and $\mathcal{C} = 2.0 \times 10^{-16}$ cm$^{-3/2}$ g$^{1/2}$ (see Appendix B), we obtain $\epsilon \approx 0.18$. This small, but not very small, value of ϵ allows for an illuminating, but not highly accurate, attack on the problem of molecular cloud core formation and collapse. In practice, turbulence within the forming core may increase the effective diffusion coefficient by a factor of several (Zweibel 2002; Fatuzzo & Adams 2002; Heitsch et al. 2004; Nakamura & Li 2005), which makes ϵ a marginally small parameter. On the other hand, if cosmic-ray fluxes are enhanced within molecular clouds (Fatuzzo et al. 2006), the value of ϵ could be reduced by a factor of several. Thus, we anticipate that ϵ might have large variations within molecular clouds, accounting in part for the wide range of observed core masses. The formal theory developed here allows a semianalytical description of only those cores that form from regions where $\epsilon \ll 1$, but we anticipate that many of the physical insights gained from the formal analysis may carry over to the more general case even when $\epsilon \sim 1$.

3.2. *Solution by Iteration*

From many numerical simulations, we know that the effect of ambipolar diffusion in cloud cores is to try to redistribute the magnetic flux from the inner region, where the flux-to-mass ratio f has a relatively low, constant value, to the outer region, where f has a relatively high, constant value. By relatively high, we mean typically $f \approx 1$; and by relatively low, we mean typically $f \approx 1/2$. Thus, f may vary only by a factor of 2 over a dynamic range in spatial scale of 10^4, say, from 10^{-4} pc to 1 pc, whereas the volume density $\propto \Sigma/2z_0$ over the same range of radii might differ by a factor of as much as 10^8 (say, from 10^{11} to 10^3 molecules cm^{-3}—to be more precise, see Fig. 7). As a consequence, it must be a good approximation to regard f to be a constant f_0 for calculations of the mechanical state of the most interesting parts of a condensing cloud core.

To justify this conclusion mathematically, define a dimensionless measure of the time by

$$\tau \equiv |t|/t_0, \tag{22}$$

where t_0 is an arbitrary unit of time used to make the argument of the logarithm dimensionless. To be definite, if we think of the core as having an outer boundary that connects to a common envelope at $\varpi_{\rm ce}$, we may choose t_0 to equal the time it takes a fast MHD wave traveling at speed $\Theta^{1/2}a$ to traverse the distance $\varpi_{\rm ce}$. In numerical terms, this would typically make $t_0 \sim 10^6$ yr. With the definition from equation (22), equation (19) becomes

$$-\frac{\partial f}{\partial \ln \tau} + (x + \tilde{v})\frac{\partial f}{\partial x} = \frac{\epsilon}{x\tilde{\sigma}^2}\frac{\partial}{\partial x}\left[x\tilde{\sigma}\tilde{b}\left(\frac{f^2}{\sqrt{1 + f^2}}\right)\right]. \tag{23}$$

We proceed now to solve the governing set of equations by an iterative process.

Begin by denoting solutions of the dynamical equations with f taken to be a fixed f_0 by the symbols $\tilde{\sigma}_0$, $\tilde{v}_0$, and $\tilde{b}_0$. With the substitution of equation (21), when $\tilde{b} = \tilde{b}_0$, it is then trivial to show that the governing equation of continuity reads

$$\left(1 + x\frac{d}{dx}\right)\tilde{\sigma}_0(x) + \frac{1}{x}\frac{d}{dx}[x\tilde{v}_0(x)\tilde{\sigma}_0(x)] = 0, \tag{24}$$

whereas the force equation becomes

$$[x + \tilde{v}_0(x)]\frac{d\tilde{v}_0}{dx} + \frac{\Theta_0}{\tilde{\sigma}_0(x)}\frac{d\tilde{\sigma}_0}{dx} = -\left(1 - f_0^2\right)\int_0^\infty K_0\left(\frac{y}{x}\right)\tilde{\sigma}_0(y)\frac{y\,dy}{x^2}, \tag{25}$$

with

$$\Theta_0 \equiv \frac{1 + 2f_0^2}{1 + f_0^2}. \tag{26}$$

Once solutions for $\tilde{\sigma}_0$, $\tilde{v}_0$, and $\tilde{b}_0$ have been found, we can return to equation (23) and replace the factor $f^2/(1+f^2)^{1/2}$ in the order ϵ diffusion term by its zeroth-order approximation $f_0^2/(1+f_0^2)^{1/2}$. We can then obtain a better estimate for f by integrating the resulting *linear* partial differential equation for f,

$$-\frac{\partial f}{\partial \ln \tau} + (x + \tilde{v}_0)\frac{\partial f}{\partial x} = \epsilon\left(\frac{f_0^3}{\sqrt{1+f_0^2}}\right)\frac{1}{x\tilde{\sigma}_0^2}\frac{\partial}{\partial x}\left(x\tilde{\sigma}_0\tilde{b}_0\right), \tag{27}$$

where we have defined

$$\tilde{b}_0(x) \equiv \int_0^\infty K_0\left(\frac{y}{x}\right)\tilde{\sigma}_0(y)\frac{y\,dy}{x^2}. \tag{28}$$

Note that the flux ratio $f = f_0$ has been removed from the definition of $\tilde{b}_0$ and is now included in the leading coefficient. In principle, one could continue to iterate solutions of the flux-to-mass distribution from the induction equation with solutions of the surface density (from which we can get the magnetic field from the flux-to-mass distribution) and velocity field from the equations governing the mass and momentum flow of the fluid to obtain increasingly accurate numerical answers to the overall problem. In practice, we stop at the perturbative step from equation (27).

3.3. *Homology and Self-Similarity*

By introducing new scaled variables, we can transform the governing ordinary integro-differential equations for the zeroth-order dynamics into a universal form that is nominally independent of the numerical value of $\lambda_0 = f_0^{-1}$. Specifically, we adopt a scaling transformation of the form

$$\xi \equiv x/\sqrt{\Theta_0}, \tag{29}$$

$$v(\xi) \equiv \tilde{v}_0(x)/\sqrt{\Theta_0}, \tag{30}$$

$$\sigma(\xi) \equiv \tilde{\sigma}_0(x)\left(1 - f_0^2\right)/\sqrt{\Theta_0}, \tag{31}$$

where the scaling coefficients are independent of x. Note that the flux ratio must obey the constraint $f_0 < 1$ (and hence $\lambda > 1$) for the surface densities σ and $\tilde{\sigma}_0$ to be positive. The scaled forms of the equation of motion then become

$$\mathcal{D}\frac{dv}{d\xi} = (\xi + v)\left(F + \frac{1}{\xi}\right), \tag{32}$$

$$\frac{\mathcal{D}}{\sigma}\frac{d\sigma}{d\xi} = -\frac{(\xi + v)^2}{\xi} - F, \tag{33}$$

where the normalized force F is defined by

$$F(\xi) = -\frac{1}{\xi^2}\int_0^\infty K_0\left(\frac{\eta}{\xi}\right)\sigma(\eta)\eta\,d\eta. \tag{34}$$

In the equations above, the discriminant $\mathcal{D}$ is given by

$$\mathcal{D} \equiv (\xi + v)^2 - 1. \tag{35}$$

It is easy to see that the normalized equations (32) and (33) are exactly what would have resulted if we had looked at the outset for self-similar solutions of the unmagnetized problem, $f_0 = 0$, $\Theta_0 = 1$. This *mathematical homology* explains the decades of confusion and controversy as to what constitutes the proper "initial conditions" for the latter type of calculations (e.g., Larson 1969; Penston 1969; Shu 1977; Whitworth & Summers 1985; Foster & Chevalier 1993; André et al. 2000). Our group (e.g., Shu et al. 1987; Lizano & Shu 1989; Li & Shu 1996) has long maintained that the pivotal *instant* $t = 0$ represents not an "initial condition" where singular conditions are reached at the origin, but rather a transitional *instant* between an extended period, $t < 0$, of magnetic evolution through flux loss via ambipolar diffusion and another period, $t > 0$, of dynamical collapse, infall, and star plus centrifugal disk formation. This paper then provides the mathematical justification for the latter point of view, and it supplies the means to select from the wealth of "extended-contraction/runaway-condensation" solutions for $t < 0$ advocated first by Hunter (1977) as worthy alternatives to Shu's (1977) choice to start at $t = 0$ with singular isothermal systems at rest, after what Shu argued would be a period of subsonic evolution to reach such a state. The corresponding static starting state here reads: $v = 0$, $\sigma = 1/\xi$, and $F = -1/\xi$, which provide exact solutions of the equations (32), (33), and (34), but not exactly those that we want here.

The critical point of the flow occurs where $\mathcal{D} = 0$. In order for the flow to pass smoothly through the critical point ξ_*, the right-hand sides of both equations (32) and (33) must vanish where $\mathcal{D} = 0$. This requirement defines two conditions, which act to fix the values of v and σ at the critical point $\xi = \xi_*$. Using L'Hôpital's rule, we can integrate inward and outward from ξ_*. We require that the inward integration satisfies the inner boundary condition $v = 0$ at $\xi = 0$. Note that only one value of ξ_* can satisfy this constraint. With the critical point thus specified, the outward integration from the same point $\xi = \xi_*$ produces the asymptotic behavior $\sigma \to A\xi^{-1}$ and $v \to v_\infty$ as $\xi \to \infty$.

3.4. *The Flux-to-Mass Distribution and Intermediate Asymptotics*

In reduced and scaled variables, the equation (27) can be written

$$-\frac{\partial f}{\partial \ln \tau} + [\xi + v(\xi)]\frac{\partial f}{\partial \xi} = -\left[\frac{\hat{\epsilon}}{\xi\sigma^2(\xi)}\right]\frac{d}{d\xi}[\xi\sigma(\xi)F(\xi)], \tag{36}$$

where we have defined

$$\hat{\epsilon} \equiv \frac{\epsilon f_0^3}{\sqrt{1+2f_0^2}}. \tag{37}$$

Note that the dependence of the overall scaled problem on the parameters ϵ and f_0 enters explicitly only in equation (36) through $\hat{\epsilon}$. In what follows, we see that the proper formulation of an initial-value problem for the solution of equation (36) will connect ϵ and f_0, i.e., that the flux-to-mass ratio of the central-most regions of a condensing cloud core depends on the dimensionless rate of ambipolar diffusion as measured by the parameter ϵ.

The linear partial differential equation (36) can be attacked by the method of characteristics:

$$\frac{df}{d\xi} = \hat{\epsilon}\mathcal{N}(\xi) \text{ on the trajectory } \frac{d}{d\xi}(-\ln\tau) = \frac{1}{\xi + v(\xi)}, \tag{38}$$

where

$$\mathcal{N}(\xi) \equiv -\frac{1}{\xi\sigma^2(\xi+v)}\frac{d}{d\xi}[\xi\sigma F(\xi)] \tag{39}$$

is regarded as a known function of ξ. Thus, we may define the formal integral,

$$N(\xi) \equiv \int_1^\xi \mathcal{N}(\xi)\,d\xi, \quad T(\xi) \equiv \int_1^\xi \frac{d\xi}{\xi + v(\xi)}, \tag{40}$$

and we write the solution to equation (36) as

$$f(\xi,\tau) = f(1,\tau_1) + \hat{\epsilon}N(\xi), \tag{41}$$

where ξ is the present position at the present time τ connected to a past (or future) position 1 at the time τ_1 on a Lagrangian trajectory that reads in similarity coordinates

$$T(\xi) + \ln\tau = \ln\tau_1. \tag{42}$$

With equation (42) giving τ_1 as a function of ξ and τ, equation (41) yields the general solution for the advection-diffusion equation (36) where the term $\hat{\epsilon}N(\xi)$ gives the effect of the ambipolar diffusion relative to a comoving observer and $f(1,\tau_1)$ gives the effect of advection if we follow the fluid motion assuming field freezing.

To illustrate the behavior of $f(1,\tau_1)$, we first note that the position $\xi = \varpi/\Theta^{1/2}at_0\tau = 1$ lies just outside the origin $\varpi = 0$ as $\tau \to 0$, whereas the same $\xi = 1$ position lies at a great radial distance ϖ in the limit $\tau \to \infty$. Thus, we have the generic behavior

$$f(1,0) = f_0, \quad f(1,\infty) = 1, \tag{43}$$

if the supercritical core connects to a marginally critical common envelope. In § 5.3, for reasonable core models we find that $N(\infty)$ is small compared to unity. [See Fig. 4 and note $N(\infty) = N_0(\infty) - N_0(1)$.] On the other hand, note that if $v(\xi)$ were zero, $T(\xi)$ would equal $\ln\xi$, and the characteristic trajectory would simply follow a line defined by $\ln(\tau\xi) = \text{const}$, i.e., a line of constant $\tau\xi = \varpi/\Theta_0 at_0$ or constant ϖ (because fluid elements are not moving if v is zero). Although the inflow velocity, $v(\xi)$, is not zero in our problem, it becomes a constant at large ξ, where the term $\xi + v(\xi)$ is dominated by ξ. The relationship between τ_1 and ξ and τ is then given by

$$\tau_1 \approx \xi\tau. \tag{44}$$

Thus, in the limit $\tau \to 0$ with $\xi \gg 1$, when the moment of gravomagneto catastrophe is approached, the flux-to-mass distribution as given by equation (41) has the approximation $f(\xi,\tau) \approx f(1,\xi\tau)$ and assumes all intermediate values between $f(1,0) = f_0$ at small $\xi\tau \propto \varpi$ and $f(1,\infty) = 1$ at large $\xi\tau \propto \varpi$. In other words, during the runaway phase of core condensation, the function $f(\xi,\tau)$ "freezes" with a profile that is a function only of the Lagrangian coordinate (which could be taken to be the enclosed cylindrical mass) varying monotonically from f_0 at the core center to unity at the outer core boundary.

Consider now a position $\xi \ll 1$ at small but finite $\tau > 0$ after runaway condensation is in progress (which occurs roughly at $\tau \sim 1$; see § 5.3), with the spacetime point (ξ,τ) being connected to an initial pair $(1,\tau_1)$ near the outer core boundary, i.e., where $f(\xi,\tau) \approx f_0$ and $f(1,\tau_1) \approx 1$. Equation (41) then requires

$$-\hat{\epsilon}N(0) = 1 - f_0. \tag{45}$$

Together with the definition from equation (37), equation (45) provides us with an eigenvalue relationship between f_0 and ϵ. In other words, for given ϵ, runaway condensation occurs when ambipolar diffusion has produced a central flux-to-mass ratio that satisfies

$$\frac{(1-f_0)\sqrt{1+2f_0^2}}{f_0^3 N_0(1)} = \epsilon, \tag{46}$$

where $N_0(1) = -N(0) = \int_0^1 \mathcal{N}(\xi)\,d\xi$ (see Fig. 4 in § 5.3).

Unfortunately, these properties of the general solution depend on the seemingly innocuous assumption that $\mathcal{N}(\xi)$ is integrable at $\xi = 0$ and ∞. However, as shown in the following sections, at small ξ the functions $\sigma(\xi)$, $v(\xi)$, and $F(\xi)$ approach the forms

$$\sigma(\xi) \to \sigma_0, \quad v(\xi) \to -\xi/2, \quad F(\xi) \to F'(0)\xi, \tag{47}$$

as $\xi \to 0$. Thus, for small ξ, $\mathcal{N}(\xi)$ behaves as

$$\mathcal{N}(\xi) = -\frac{4F'(0)}{\sigma_0\xi} \quad \text{for} \quad \xi \ll 1. \tag{48}$$

In these circumstances, $N(\xi,\tau)$ will diverge as $[4F'(0)/\sigma_0]\ln\xi$ as $\xi \to 0$. The divergence arises because in the derivation for the average value of $\mathcal{C}^{-1}$ in equation (B3), we have set $\partial B_\varpi/\partial z$ equal to $(B_\varpi^+/z_0)\mathrm{sech}^2(z/z_0)$. This approximation is valid away from the origin, but at the origin, $\partial B_\varpi/\partial z$ is doubly small, because not only $B_\varpi \propto B_\varpi^+$ itself is small, but the magnetic field is vertical near the origin so $\partial/\partial z$ is also small. The replacement of $\partial B_\varpi/\partial z$ by something proportional to $B_\varpi^+/z_0 \propto \sigma(\xi)F(\xi)$ accounts for the first effect, but not the second.

As a related point, the current density $\propto(\partial B_\varpi/\partial z - \partial B_z/\partial\varpi)$ is dominated at the origin, not by $\partial B_\varpi/\partial z$, but by $\partial B_z/\partial\varpi$, implying that the Lorentz force there comes mostly from the gradient of the "magnetic pressure" $-\partial(B_z^2/8\pi)/\partial\varpi$ rather than from the "magnetic tension" $(B_z/4\pi)\partial B_\varpi/\partial z$. This dominance is evident in that it is the pressure (gas plus magnetic) that decelerates the inflow to rest at the origin, not the tension (see eq. [73]). The transition in roles of the tension versus the pressure when one moves from the disk of the core to its central regions has implications for the ambipolar diffusion that occurs near the origin, which the unadulterated diffusion term $\mathcal{N}$ in equation (39) does not treat correctly. Indeed, near the origin, the diffusion term involves the second derivative $\partial^2 B_z/\partial\varpi^2$ that translates into a term proportional to $\partial^2(\sigma f)/\partial\xi^2$. In a rigorous discussion, we would examine the central regions anew and provide a proper matching of the

solutions there with those applicable for the more highly flattened regions of the cloud core developed here. The extra radial derivative that appears via $\partial^2(\sigma f)/\partial\xi^2$, multiplied by a small coefficient ϵ, makes possible asymptotic matching of the inner solution to an outer or intermediate solution. In particular, it would be possible to invoke an extra boundary condition, say, $\partial f/\partial\xi = 0$, at the origin to ensure that f is well behaved at the origin. A formal attack along these lines would involve singular perturbation theory, coupled with the introduction of multiple length scales and/or timescales (Bender & Orszag 1978).

In other words, our problem is really one of *intermediate asymptotics* (Barenblatt 1996). A proper treatment would asymptotically match the intermediate core on an outer scale to a common envelope, where the assumption of gravitational contraction breaks down. It would do the same on an inner scale to the central region, where the assumption of a flattened configuration is invalid. For the sake of physical clarity, we forego such a formal study in this paper and join the intermediate core to a common envelope only in terms of its magnetic connection and not in terms of mechanical considerations. We also incorporate the region near the origin into the intermediate analysis by fixing the problem presented above, as well as one that will appear below, with simple procedures that are physically rather than mathematically motivated. We defer to § 5.3 therefore our prescription for making $\mathcal{N}(\xi)$ regular at the origin.

4. SHEET CONDENSATION SOLUTION

4.1. *Gravity Formulation in Terms of the Enclosed Mass*

In order to obtain an approximation to the condensation solution for $t < 0$, we can make the assumption that the potential is given by the monopole associated with the enclosed mass. Although it is possible to develop this approximation as the first term of a general multipole expansion (see Appendix E), we prefer a motivation based on physical intuition. We start by defining the cylindrically enclosed mass $M(\varpi, t)$ in dimensional units,

$$M(\varpi, t) = \int_0^{\varpi} 2\pi r\, dr\, \Sigma(r, t). \tag{49}$$

The statement that the enclosed mass is conserved if we follow the motion of mass annuli,

$$\frac{\partial M}{\partial t} + u\frac{\partial M}{\partial \varpi} = 0, \tag{50}$$

may be regarded as an integrated form of the continuity equation (1). If we use the dimensionless variables defined by equations (12), then equations (49) and (50) become

$$M(\varpi, t) = \frac{a^3}{G}|t|\tilde{m}(x), \quad \text{where} \quad \tilde{m}(x) = \int_0^x \tilde{\sigma} x\, dx, \tag{51}$$

$$-\tilde{m} + (x + \tilde{v})\frac{d\tilde{m}}{dx} = 0, \tag{52}$$

where we have assumed the case where $t < 0$. We employ the same scaling transformation as before (see eqs. [29]–[31]) to express the equations in terms of the variables ξ, v, and σ. The dimensionless enclosed mass now becomes

$$\tilde{m}(x) = \frac{\Theta_0^{3/2}}{1 - f_0^2} m(\xi), \quad \text{where} \quad m(\xi) \equiv \int_0^{\xi} \sigma\xi\, d\xi. \tag{53}$$

The differential version of the last equation,

$$\frac{dm}{d\xi} = \xi\sigma, \tag{54}$$

may be combined with the scaled version of equation (52),

$$m = (\xi + v)\frac{dm}{d\xi} = \xi(\xi + v)\sigma, \tag{55}$$

to express the monopole approximation for the force in the form

$$F(\xi) = -\frac{m}{\xi^2} = -\frac{1}{\xi}(\xi + v)\sigma. \tag{56}$$

As a check, note that ξ times the equation of continuity, written in the usual fashion as the scaled version of equation (24),

$$\xi\frac{d}{d\xi}(\xi\sigma) + \frac{d}{d\xi}(\xi\sigma v) = -\xi\sigma + \frac{d}{d\xi}[(\xi + v)\xi\sigma] = 0, \tag{57}$$

is simply the derivative of equation (55) with respect to ξ. With the force F reduced to a local expression, equations (32) and (33) become the following coupled set of first-order, nonlinear ordinary differential equations:

$$\mathcal{D}\frac{dv}{d\xi} = \frac{(\xi + v)}{\xi}[1 - \sigma(\xi + v)], \tag{58}$$

$$\mathcal{D}\frac{d\sigma}{d\xi} = (\xi + v)\frac{\sigma}{\xi}[\sigma - (\xi + v)], \tag{59}$$

where the discriminant $\mathcal{D}$ is given by equation (35).

4.2. *Critical Points*

At the critical points ξ_*, $\mathcal{D} = 0$, so the right-hand sides of equations (59) and (58) must also vanish. This condition thus determines the value of the density field at the critical point,

$$\sigma(\xi_*) = 1. \tag{60}$$

If we expand around the critical point, the leading-order corrections have the forms

$$\xi = \xi_* + \delta\xi, \quad v = v_* + v_1\delta\xi, \quad \sigma = \sigma_* + \sigma_1\delta\xi. \tag{61}$$

Using these expressions in the equations of motion and keeping only the leading-order terms, we can find the field derivatives at the critical point,

$$v_1 = -\frac{1}{2} \pm \frac{1}{2\xi_*}\left[(\xi_* - 1)^2 + 1\right]^{1/2},$$

$$\sigma_1 = \frac{1}{2\xi_*}\left\{\xi_* - 2 \mp \left[(\xi_* - 1)^2 + 1\right]^{1/2}\right\}. \tag{62}$$

Appendix D generalizes this procedure for arbitrary forms of $F(\xi)$.

4.3. *Limiting Forms*

In the limit $\xi \to \infty$, the force equation allows for an asymptotic solution for the surface density, namely,

$$\sigma = A/\xi, \tag{63}$$

where A is a constant. With this form for the surface density, the asymptotic behavior for the velocity can be found,

$$v(\xi) \to v_\infty + \frac{A-1}{\xi}, \tag{64}$$

where v_∞ is a constant. The second correction term goes to zero as $\xi \to \infty$, but the falloff is slow. As a result, the inflow velocity will in general be nonzero but small even at the pivotal instant of gravomagneto catastrophe (Allen et al. 2003; Fatuzzo et al. 2004); this result, in turn, implies that the subsequent infall rates will be larger than for cases where the starting states are in exact hydrostatic equilibrium.

In the limit $\xi \to 0$, we want to enforce the boundary conditions

$$v \to 0, \quad \sigma \to \sigma_0 = \text{const.} \tag{65}$$

The solution for the velocity field near $\xi = 0$ has the dependence

$$v(\xi) = -\frac{1}{2}\xi. \tag{66}$$

With this limiting expression for v, the density field takes the form

$$\sigma(\xi) = \frac{\sigma_0}{1 + \sigma_0 \xi/2}. \tag{67}$$

Note that this particular function becomes $\sigma = 2/\xi$ at large values of the scaled similarity variable ξ, whereas the asymptotic limit of the density field has the form $\sigma = A/\xi$.

Unfortunately, the behavior near the origin is less than perfect in a model of starless cloud cores as flat sheets. The monopole associated with a sheet produces a net scaled force (gravitational plus magnetic tension) that approaches the form $F \to -\sigma_0/2 = -2.524$ as $\xi \to 0$ (see eq. [56] and below). The origin of this behavior rests with the unscaled reduced force behaving as $\tilde{F} = -(1 - f_0^2)\tilde{m}_0/x^2$ with $\tilde{m}_0 = \tilde{\sigma}_0 x^2/2$ if the surface density approaches a constant $\tilde{\sigma}_0$ in the limit $x \to 0$. In other words, with constant surface density, the mass enclosed within a cylindrical radius scales as the square of that radius, which cancels the inverse square law of Newtonian gravity for monopoles (and Ampérian magnetism for split monopoles). Hence, unlike the classic freshman physics problem of the gravitational field inside a sphere of uniform volume density, the corresponding force in an axisymmetric flat sheet of uniform surface density does not go to zero, even when we approach the origin!

However, by symmetry considerations, the radial force must vanish right at the origin for any axisymmetric mass and current distribution that is regular there. Appendix E shows that a jump in the physical behavior as one changes from being at the origin to being slightly off it is generic to *any* order in a general multipole expansion of an axisymmetric sheet. On the other hand, incompletely flattened, magnetized, isothermal disks/toroids have scaled reduced half-height ζ_0 and dimensionless *volume* density of the form $\alpha = (\sigma/2\zeta_0)\mathrm{sech}^2(\zeta/\zeta_0)$ (see Appendix A). If the volume density is regular at $\xi = 0$ (rather than diverging as ξ^{-2}, which applies only at the pivotal instant $t = 0$), then $F \propto \xi \to 0$ as $\xi \to 0$ (see Appendix F). Accounting for the finite thickness of actual molecular cloud cores thus cures the unphysical situation at the origin. As a result, a solution that enforces physical boundary conditions at the origin based on the fluid's reaction to a *sheet* monopole is clearly blemished. In the interest of obtaining practical and useful results, however, we defer further discussion of this imperfection until § 5.

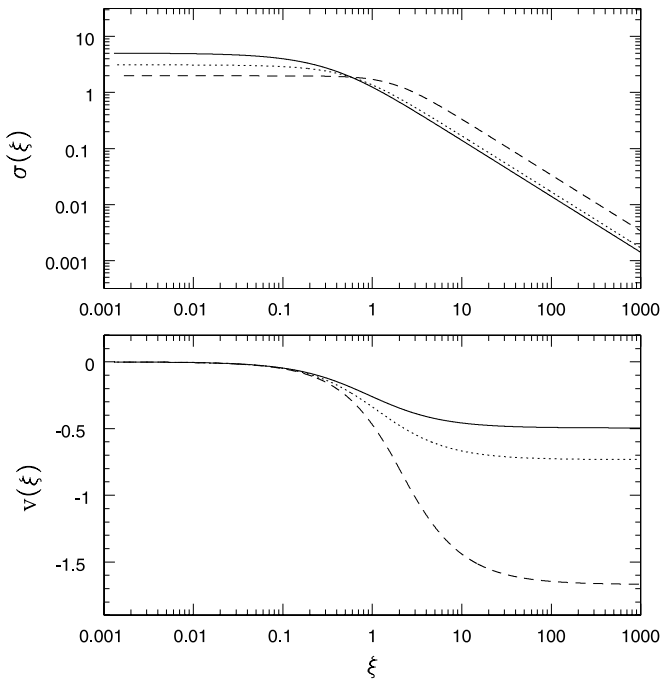

FIG. 1.—Reduced fluid fields for the pure monopole, monopole plus quadrupole, and full sheet solutions plotted, respectively, as the solid, dotted, and dashed curves. The solutions for reduced and scaled surface density $\sigma(\xi)$ and velocity $v(\xi)$ are given, respectively, by the top and bottom panels, with the limiting values $\sigma \to \sigma_0$ and $v \to 0$ as $\xi \to 0$; $\sigma \to A/\xi$ and $v \to v_\infty$ as $\xi \to \infty$. The parameter values are tabulated in Table 1.

4.4. *Sheet Monopole Solution*

With the preliminaries in place, we can now find the critical points and integrate both inward toward $\xi = 0$ and outward to large ξ to find the solutions for the reduced and scaled density and velocity fields (in this monopole approximation). In the usual case, these two coupled ordinary differential equations would require two boundary conditions to specify a solution. In this setting, equations (65) supply the inner boundary conditions on v and σ, but we do not know the correct value σ_0 to enforce. However, this problem contains an additional constraint, namely, that the flow must pass smoothly through the critical point ξ_* (specifically, the fluid fields v and σ must be continuous at ξ_*, but their derivatives need not be). Since each starting value of σ_0 would lead to a different value of σ at the critical point, only one value σ_0 allows for smooth flow. To find this value, we start the integration at a possible critical point and integrate inward toward $\xi = 0$. By requiring that the solution satisfy the inner boundary condition on v, we can iterate the starting point until we find the correct value of the critical point. With this value specified, we then integrate outward from the critical point. With no further quantities to specify, this integration thus determines both A and v_∞. The resulting solution is shown in Figure 1 (along with solutions from § 5).

The solutions for v and σ follow the limiting forms found analytically in § 4.3. From the numerical solution, we can find the values of the parameters appearing in the analytic forms: $\xi_* = 1.294$, $\sigma_0 = 5.03$, $A = 1.40$, and $-v_\infty = 0.495$. We can combine the inner and outer limiting forms for the density profile to construct an approximate solution,

$$\sigma_A(\xi) = \left(\frac{\sigma_0}{1 + \sigma_0 \xi/2}\right)\left(\frac{1 + A\xi/2}{1 + \xi}\right), \tag{68}$$

that agrees well with the numerical solution with an rms error over the range of ξ shown in Figure 1 of only $\sim$1%. Similarly, we can fit the velocity field with the form

$$v_A(\xi) = \frac{v_\infty \xi}{\xi + 2|v_\infty|}, \tag{69}$$

where this result agrees with the numerical solution with an rms error of $\sim$2%.

One of the most important quantities resulting from this calculation is the value of the nonzero velocities in precollapse cores, i.e., cores that have not yet produced protostars at their centers. The physical value of this inward speed is given by $u_\infty = a v_0(\xi \to \infty) = a v_\infty (\Theta_0)^{1/2}$. Since the flux-to-mass ratio f_0 must lie in the range $0 \le f_0 \le 1$, the correction parameter Θ_0 is confined to the range $1 \le \Theta_0 \le 3/2$. As a result, the head start velocity is constrained to lie in the range

$$0.495 \le -\frac{u_\infty}{a} \le 0.606, \tag{70}$$

where a is the isothermal sound speed (and the minus sign denotes inward velocities). These values are consistent with, although perhaps slightly smaller after projection than, the extended infall velocities observed in starless molecular cloud cores (e.g., Lee et al. 2001; Harvey et al. 2002).

Another important physical quantity in this problem is the size of the region of nearly constant density in the core center. The similarity solution (Fig. 1) shows that the surface density σ has zero slope in the center and steepens to the form $\sigma = A/\xi$ in the outer regime. We can thus define the outer boundary of the core region to be the location where the index $p \equiv -(\xi/\sigma)(d\sigma/d\xi) = 1/2$. Using the approximate form given by equation (68), we find that the outer boundary of the core region occurs at $\xi_{1/2} \approx 0.313$. The physical location of this boundary is given by

$$\varpi_{1/2} \approx 0.313 a |t| \sqrt{\Theta_0}, \tag{71}$$

where the column density falls to 0.519 of its central value.

To summarize, before $t = 0$, condensing, magnetized molecular cloud cores display a finite region of nearly constant central surface density that makes them mimic static Bonnor-Ebert spheres. In actuality, however, the surrounding regions of the core are in a state of extended contraction at a significant fraction of the isothermal sound speed a. In the limit $t \to 0^-$, this central region loses its finite extent and the core attains a pure power-law configuration, $\Sigma \propto \varpi^{-1}$, that corresponds ideally in three dimensions to a flattened singular isothermal toroid, $\rho \propto r^{-2} R(\theta)$ in spherical polar coordinates. The core subsequently goes into true dynamical collapse onto a central protostar.

5. BEYOND THE SHEET MONOPOLE APPROXIMATION

Before we consider the collapse solution for $t > 0$ (see § 6), we consider the three shortcomings in our treatment of the gravity of a flattened core by the sheet monopole approximation.

1. For a flattened core, the monopole approximation represents only the first term in a more general multipole expansion (see Appendix E). These higher multipole terms convey two types of corrections. Inner multipoles correct for the fact that matter in a flat sheet interior to the field point ξ is (on average) closer to ξ than if the enclosed mass were placed at the core center. Outer multipoles correct for the gravitational pull of the matter in the sheet outside of the field point ξ. The physical description for the action of currents is more complicated, because we have used a scalar potential rather than the vector potential to describe the magnetic field (see Li & Shu 1997), but the consequence for the magnetic tension is the same except the tension force acts in opposition to self-gravity.

2. The aspect ratio, which is given by

$$\frac{z_0}{\varpi} = \frac{2}{(1+f_0^2)x\tilde{\sigma}} = \left[\frac{2(1-f_0^2)}{1+2f_0^2}\right]\left(\frac{1}{\xi\sigma}\right), \tag{72}$$

cannot be small compared to unity in the limit $\xi \to 0$. Indeed, even at large ξ, $z_0/\varpi = 2(1-f_0^2)/A(1+2f_0^2)$, which equals $1.4(1-f_0^2)/(1+2f_0^2)$ for the sheet monopole solution, and is not small unless f_0 is close to unity. The assumption that the cloud core is highly flattened is egregiously violated in the central regions, precisely where the surface density profile flattens instead of continuing inward as $\sigma = A/\xi$. For the monopole solution, at $\xi = \xi_{1/2}$ we have $z_0/\varpi = 2.44(1-f_0^2)/(1+2f_0^2)$, which has a value 1.22 for a typical $f_0 = 1/2$.

3. The regions at large ξ are not fully isopedic with constant $f = f_0$ (see § 5.3). If f is an increasing function of ξ, then the force of magnetic tension becomes increasingly strong relative to the force of self-gravity, instead of maintaining a constant ratio (with opposite signs), as is true in the inner core. Growing magnetic support against self-gravitation as the envelope is approached will presumably also reduce the induced inflow velocities.

We now discuss how these shortcomings may affect a peculiar aspect of the sheet monopole solution obtained in § 4. We found that the flow properties are completely defined by the behavior of the gas near the origin $\xi = 0$. In particular, Appendix C proves that the velocity profile is monotonic, which implies that if inflow occurs at any point in the self-similar system, then (for $t < 0$) the flow must pass through a critical point where $v = 1 - \xi$ and approach the form $v = -\xi/2$ near the origin. The latter behavior during the cloud core condensation stage has nothing to do with gravitational minus tension forces. It represents the deceleration of an initially inwardly directed velocity by the pressure forces. Independent of how the force F behaves, as long as it does not diverge at the origin, equation (32) implies at small ξ,

$$(-1)\frac{dv}{dx} = \frac{1}{\xi}(\xi + v), \tag{73}$$

where the -1 remaining in the discriminant comes from the pressure gradient. The above equation has the solution $v = -\xi/2$ if the velocity v vanishes at the origin.

In itself, the above result is not particularly ominous. But smooth passage through the critical point also determines the solution that is reached at asymptotic infinity, in particular, the values of the head start velocity v_∞ and the surface density coefficient A. How is it possible for the conditions near the center of a condensing cloud core to dictate how the core connects at asymptotic infinity to the cloud envelope? Is that not putting the cart before the horse? In principle, if there is enough time and the inflow is submagnetosonic, as is the case with the monopole solution, then one could imagine the central regions to have a magnetohydrodynamic influence on the outer regions. However, we are not guaranteed such simple behavior in every circumstance, and naive treatments of the core gravity can produce supermagnetosonic condensation speeds (see below). Would not such solutions be unstable to shock formation as the pressure forces attempt to bring the inflow to a halt at the core center? (Compare this question with previous criticism [Shu 1977] of the Larson-Penston solution, which is overdense and supersonic by even larger margins, and the placement of

the Larson-Penston solution in the context of *champagne* outflows [Shu et al. 2002].)

Slow core condensation by ambipolar diffusion avoids the above paradox. As flux is lost from the central regions to the outer regions above (to reach typical values of $f_0 \approx 1/2$), the inner core begins a stage of extended contraction at a fraction of the magnetosonic speed—as is seen in both numerical simulations (e.g., Basu & Mouschovias 1994) and observations (e.g., Lee et al. 2001; Harvey et al. 2002). If the leakage of the flux is slow, as it must be because the envelope of a typical molecular cloud is too well ionized to allow rapid motion of neutrals past ions, then the condensing core never loses so much support that its surface density coefficient in the outer parts becomes substantially greater than the equilibrium value $A = 1$. Without large overdensities $A - 1$, it is not possible to generate large head start velocities v_∞—unless one has an overidealized force calculation for $F(\xi)$ in the central regions by assuming the region is highly flattened when it is not.

With the above comments in mind, we extend the flattened monopole approximation by two different methods. In the first method, we retain the sheet approximation but compute the force in its full form (see Appendix E),

$$F(\xi) = \int_0^\infty K_0\left(\frac{\eta}{\xi}\right)\left[\frac{A}{\eta} - \sigma(\eta)\right]\eta\, d\eta - \frac{A}{\xi}, \qquad (74)$$

which is mathematically identical to equation (34). The difference surface density $A/\eta - \sigma(\eta)$ is everywhere positive, but rapidly goes to zero much outside of the central core $\eta \gg \xi_{1/2}$. Hence, the integral may be truncated at a reasonable upper limit without compromising numerical accuracy. Appendix D gives a formal description of the solution procedure for such arbitrary forms of $F(\xi)$.

In the second method, we retain the interior monopole approximation, but compute the force in a modified form. We begin by defining the reduced scaled half-thickness

$$\frac{z_0}{\Theta_0^{1/2} a|t|} = \left[\frac{2\left(1 - f_0^2\right)}{1 + 2f_0^2}\right]\frac{1}{\sigma(\xi)} \equiv \zeta_0(\xi). \qquad (75)$$

We then replace ξ in the denominator of equation (56) by $[\xi^2 + \zeta_0^2(\xi)]^{1/2}$ on the heuristic basis that the latter is a truer measure of the distance between the field point and a typical interior source point in an incompletely flattened cloud core. The softened monopole force $F(\xi)$ now reads

$$F(\xi) = -\frac{\sigma(\xi + v)}{\sqrt{\xi^2 + \zeta_0^2(\xi)}}. \qquad (76)$$

Note that equation (76) produces a force law that is proportional to ξ for small ξ, where $v \approx -\xi/2$ and $\sigma \approx \sigma_0$. Note also that the homology with unmagnetized systems has disappeared; cases with different f_0 produce different reduced scaled variables. In partial compensation, forces of the form of equation (76) are directly integrable by a slight modification of the method discussed in § 4. Finally, note that the implied "enclosed mass" no longer corresponds to the cylindrical value, because in a quasi-spherical geometry, it is more appropriate to consider a central region with constant *volume* density, which still integrates to a constant surface density in the complete vertical direction, but does not behave at small ξ as a sheet of matter and current.

5.1. *Full-Gravity Corrections in a Sheet*

The case when $F(\xi)$ is the full gravity of a sheet is shown as the dashed line in Figure 1. Note that the solution has basically the same form as the sheet monopole solution (*solid curves*), but exhibits somewhat different values of the defining constants. The critical point in the flow shifts outward to $\xi_* \approx 1.714$; the central density σ_0 becomes a somewhat smaller 1.98, while the asymptotic density coefficient A increases to 3.43, resulting in the larger (supermagnetosonic) head start speed $-v_\infty \approx 1.67$. For reference, the intermediate case for the monopole plus quadrupole corrections in a sheet geometry is plotted as dotted curves. We may attribute the full-gravity and monopole-plus-quadrupole results to net inward gravitational fields that have increased in the outer regions and decreased in the central regions relative to a pure monopole.

5.2. *Softened Monopole Gravity*

Unfortunately, the approach of § 5.1 has its own difficulty in the central regions, because the approximation that the disk is geometrically thin leads to an unphysical, nonvanishing force $F(\xi)$ near the origin before a protostar has formed there. Equation (74) shows explicitly how tricky it is even to conclude that $F(\xi)$ equals a constant at the origin rather than diverging as $1/\xi$ when we model a cloud core with a power-law envelope and a nonsingular center as a flat sheet.

The behavior at asymptotic infinity for the softened monopole is similar to the sheet monopole, but it is somewhat different near the origin. The velocity field has the same form as before, i.e.,

$$v \to -\frac{1}{2}\xi \quad \text{as} \quad \xi \to 0. \qquad (77)$$

The density field approaches the form

$$\sigma(\xi) = \sqrt{c_0}\left[1 - \left(1 - c_0/\sigma_0^2\right)e^{-\xi^2/4}\right]^{-1/2}, \qquad (78)$$

where we have defined

$$c_0 = \left(1 - f_0^2\right)/\left(1 + 2f_0^2\right). \qquad (79)$$

Note that, instead of a finite value, the gas pressure gradient is now zero at the origin, reminiscent of quasi-hydrostatic equilibrium.

Figure 2 shows the different approximations for the force prescription used in this paper. The dashed curve shows the force law for the case of full sheet gravity. Since its force changes sign at small ξ (the net force as $\xi \to 0$ is constant but directed *outward*), we cannot display the innermost region in a log-log plot. The dotted curve shows the force profile resulting from the sheet monopole approximation for the same surface density and velocity profile that resulted from the case for the full sheet gravity. This normalization is needed to make a fair comparison of the three techniques. Note that the sheet monopole force approaches a constant value (now directed *inward*) in the limit $\xi \to 0$, which leads to the difficulties discussed above. Finally, the solid curve shows the force profile calculated using the same rules but with the softened monopole approximation for the case $f_0 = 0.5$. By construction, its force law has a linear form at small ξ, vanishing at the origin, and then joins onto the standard profile at larger values of ξ.

To study the possible range of head start velocities and to assess the meaning of the artificially inflated values resulting from the anomalies of all forms of sheet gravity at the origin, we use the modified monopole prescription of equation (76) to find additional condensation solutions. The resulting solutions can also be characterized by the parameters σ_0, A, and $-v_\infty$, which are tabulated in Table 1 for varying values of f_0. Figure 3 plots the associated functions $\sigma(\xi)$ and $v(\xi)$. Note that as the dimensionless flux-to-mass ratio f_0 decreases, the degree of softening becomes larger, the effective scale height of the density distribution in the radial direction

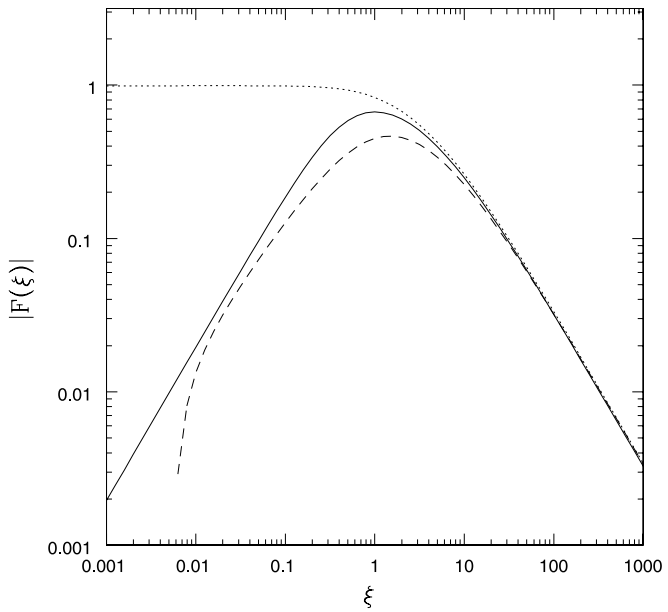

FIG. 2.—Comparison of the force profiles calculated from the full sheet gravity (*dashed curve*), the sheet monopole approximation (*dotted curve*), and the softened monopole treatment using $f_0 = 1/2$ (*solid curve*). For a fair comparison, all three force profiles are calculated using the same surface density and velocity as obtained in § 5.1.

becomes larger, and the critical points of the flow move outward. The flow solutions in the outer regime are specified by the parameters v_∞ and A, which grow larger with decreasing f_0. The softer gravity allows for more extended density profiles (and hence larger A) and pulls inward less strongly to allow for greater head start velocities v_∞ (see Table 1 and Fig. 3). The important point, however, is that the head start speed $-v_\infty$ in each case is *sub-magnetosonic* (i.e., $|v_\infty| < 1$).

Note also that in the limit $f_0 \to 1$, the softening parameter $\zeta \to 0$, and we recover algebraically the unsoftened monopole approximation. As a result, the $f_0 \to 1$ solution agrees with the original monopole solution (see Fig. 3 and Table 1). This case is to be regarded as the limiting case where $f_0 \to 1$ from *below*. In this limiting procedure, the weak effective gravity is compensated by the large dimensional surface density and thus produces roughly the same collapse timescale (see eqs. [88] and [99]), $M_{\rm core}/\dot{M} = (A/m_0)(\varpi_{\rm ce}/\Theta^{1/2}a)$ for cores with different values of f_0.

Since a realistic treatment should include both of the effects discussed in this subsection and § 5.1, we expect the actual results for σ_0, A, and $-v_\infty$ to be given by a combination of the two types of models. Regarding this issue, one should remember that the first three entries in Table 1 refer to the *same* sheet model; for this first model type, the full sheet gravity case is nominally the most complete (excluding the central regions of the core). Models of the second type are characterized by their f_0 values, which vary from $f_0 = 0$ for the unmagnetized spherical limit to $f_0 = 1$ for the highly flattened, critically magnetized case. For $f_0 = 1$, the disk thickness and the "softening" due to it disappear, and the softened monopole becomes identical to the sheet monopole, i.e., they both lack the full complement of higher multipoles that is present implicitly in the full sheet gravity model. Nevertheless, when $f_0 \neq 1$, Figure 2 indicates that the softened monopole model mimics well the best characteristics of the full sheet gravity model while adopting none of its pathologies near the origin. For astrophysical applications, we thus regard the results presented in the bottom five rows of Table 1 to be more reliable than those of the

TABLE 1
PARAMETERS FOR DIFFUSION EPOCH SOLUTIONS

Model	ξ_*	σ_0	$-v_\infty$	A
Monopole	1.294	5.03	0.495	1.40
Quadrupole	1.407	3.12	0.732	1.68
Full Sheet Gravity	1.714	1.98	1.67	3.43
$f_0 = 0.0$	1.467	3.08	0.833	2.35
$f_0 = 0.25$	1.455	3.04	0.815	2.21
$f_0 = 0.50$	1.393	3.22	0.684	1.83
$f_0 = 0.75$	1.328	3.85	0.556	1.52
$f_0 = 1.00$	1.294	5.03	0.495	1.40

top three rows. For any of these cases, the associated surface density and velocity field may be reasonably approximated with the fitting formulae from equations (68) and (69) for $\sigma_A(\xi)$ and $v_A(\xi)$.

5.3. *Attachment of Condensing Core to Common Envelope*

We now address the solution for flux-to-mass ratio $f(\xi, \tau)$. Note that it is possible to discuss the effects of ambipolar diffusion only for the softened monopoles of § 5.2 where we have made sure that $F(\xi)$ goes linearly to zero as $\xi \to 0$. The magnetic tension force $\propto -f_0^2 F(\xi)$ acts on the ions (but not the neutrals) and drives ambipolar diffusion via the term $\mathcal{N}$ in equation (38). This term would be badly divergent at the origin if $F(\xi)$ went to a constant there, rather than vanishing as a linear function of ξ. As it is, however, the integral of $\mathcal{N}$ is still logarithmically divergent, as already discussed in § 3.4. To make $\mathcal{N}$ even better behaved, without a lot more analysis, which would be an onerous investment when weighed against the limited enlightenment such an effort would yield, we adopt the simple procedure of modifying $\mathcal{N}$ in the following manner.

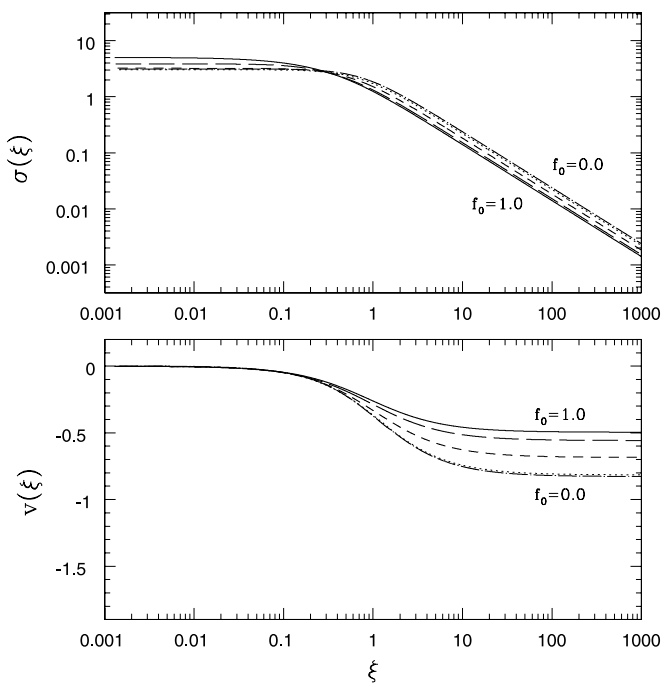

FIG. 3.—Reduced fluid fields for the softened monopole solutions. The velocity field is shown in the bottom panel, and the density field is shown in the top panel. In each case, the curves correspond to varying degrees of softening, as determined by the zeroth-order flux-to-mass ratio: $f_0 = 1$ (*solid curves*), 0.75 (*long-dashed curves*), 0.50 (*dashed curves*), 0.25 (*dotted curves*), and 0.0 (*dot-dashed curves*).

Consider anew the derivation of Appendix B, but include from the start the entire current,

$$\frac{\partial B_z}{\partial t} + \frac{1}{\varpi}\frac{\partial}{\partial \varpi}(\varpi B_z u) = \mathcal{D}, \tag{80}$$

where

$$\mathcal{D} \equiv \frac{1}{\varpi}\frac{\partial}{\partial \varpi}\left[\frac{\varpi B_z^2}{4\pi\gamma\rho\rho_i}\left(\frac{\partial B_\varpi}{\partial z} - \frac{\partial B_z}{\partial \varpi}\right)\right]. \tag{81}$$

We replace $\partial B_\varpi/\partial z$ by $(B_\varpi^+/z_o)\mathrm{sech}^2(z/z_0)$ and $\partial B_z/\partial\varpi$ by $2\pi G^{1/2}\partial(f\Sigma)/\partial\varpi$. Thus, where we see B_ϖ^+ we need to add $-z_0 f_0 \partial\Sigma/\partial\varpi$ times some coefficient that represents a thickness correction factor. In net, the modified form for the diffusion source term can now be written as

$$\mathcal{N}_{\rm L} = -\frac{1}{\xi\sigma^2(\xi+v)}\frac{d}{d\xi}\left\{\xi\sigma\left[\mathcal{M}F + \mathcal{S}\left(\frac{1-f_0^2}{1+f_0^2}\right)\frac{1}{\sigma}\frac{d\sigma}{d\xi}\right]\right\}, \tag{82}$$

where $\mathcal{M}$ and $\mathcal{S}$ are correction factors, respectively, to relate B_ϖ^+ to $-F$ and $z_0\partial B_z/\partial\varpi$ to $[(1-f_0^2)/(1+f_0^2)]\sigma^{-1}\,d\sigma/d\xi$ approximately at the origin. Although a proper treatment would require a procedure of singular perturbation theory of the type described in § 3.4, we bypass such an involved treatment by the simple act of choosing $\mathcal{M}$ and $\mathcal{S}$ to be the same thickness modification factor that we used to regularize F,

$$\mathcal{M} = \frac{\xi}{\sqrt{\xi^2+\zeta^2(\xi)}} = \mathcal{S}. \tag{83}$$

With this procedure, $\mathcal{N}_{\rm L}$ goes to a constant at $\xi = 0$ rather than diverging as $1/\xi$ near the origin. With $\mathcal{N}_{\rm L}$ replacing $\mathcal{N}$, we evaluate the integral

$$N_0(\xi) \equiv \int_0^\xi \mathcal{N}_{\rm L}(\xi)\,d\xi. \tag{84}$$

The resulting functions for $N_0(\xi)$ are shown in Figure 4 for the zeroth-order flux ratios $f_0 = 0.25$, 0.50, and 0.75. We note that the numerical values for $N_0(1)$ are 18.6, 31.1, and 77.4 for the cases $f_0 = 0.25$, 0.50, and 0.75, respectively. Furthermore, the values of $N_0(\infty)$ are nearly equal to those of $N_0(1)$, with differences of only ~2%. We denote the value of $N_0(1)$ as a function of f_0 by the symbol $I(f_0)$, and we rewrite equation (46) to obtain the following explicit relationship between ϵ and f_0:

$$\epsilon = \frac{(1-f_0)\sqrt{1+2f_0^2}}{f_0^3 I(f_0)}. \tag{85}$$

Note that the correlation of ϵ with f_0 is extremely sensitive. Specifically, in order to obtain flux-to-mass ratios $f_0 = 0.75$, 0.50, and 0.25, the required values of ϵ are 0.0112, 0.157, and 2.73, respectively. We cannot obtain a consistent approximation with $\epsilon \ll 1$ in this formulation when f_0 becomes too low. Conversely, we may say that for standard values of ϵ (≈0.18), runaway core condensation occurs typically when f_0 reaches 0.5, as indicated by simulations performed by many different groups and under very different assumptions (e.g., Nakano 1979; Lizano & Shu 1989; Basu & Mouschovias 1994). Values of f_0 appreciably smaller than 0.5 require anomalously large values of ϵ, under which the condensation problem becomes highly dynamic and can hardly be considered diffusive. Such cases, if they exist, need alternative treatments to the one given here. As indicated by

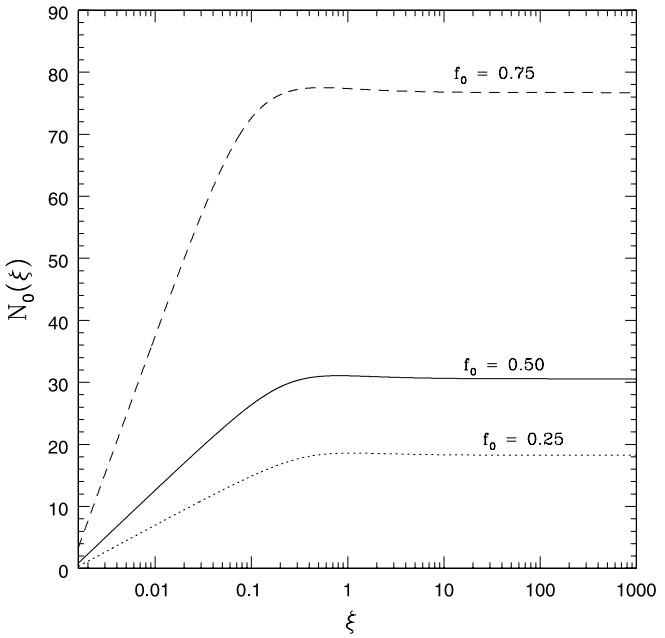

FIG. 4.—Integral $N_0(\xi)$ as a function of ξ. The three curves correspond to different values of the zeroth-order flux-to-mass ratio: $f_0 = 0.75$ (*dashed curve*), 0.50 (*solid curve*), and 0.25 (*dotted curve*).

equation (85), the limiting cases $f_0 = 0$ (spherical unmagnetized core) and $f_0 = 1$ (completely flattened, critically magnetized core) are special in that the first cannot sensibly attach onto a critically magnetized envelope unless ϵ is infinite, whereas the second loses flux from its central regions and becomes inconsistent with the assumption that $f_0 = 1$, the same value as the common envelope, unless ϵ is zero.

Although our derivation of the important equation (85) was carried out for a very specific model, we believe that the result is robust. Indeed, the result is almost given by dimensional analysis, except we do it through a dimensionless argument. Consider the vector induction equation with ambipolar diffusion as it is given by equation (27.12) of Shu (1992),

$$\frac{\partial \boldsymbol{B}}{\partial t} + \nabla\times(\boldsymbol{B}\times\boldsymbol{u}) = \nabla\times\left\{\frac{\boldsymbol{B}}{4\pi\gamma\mathcal{C}_{\rm local}\rho^{3/2}}\times[\boldsymbol{B}\times(\nabla\times\boldsymbol{B})]\right\}, \tag{86}$$

where we have specialized to the ionization law $\rho_i = \mathcal{C}_{\rm local}\rho^{1/2}$ (Appendix B). When applied to the core formation problem, the right-hand side of equation (86) is proportional to three powers of $\boldsymbol{B}$ and inversely to the product $\gamma\mathcal{C}_{\rm local}$. In dimensionless form, the right-hand side is proportional to ϵf_0^3 in the central regions of a condensing core. The left-hand side measures the distance (in time or distance divided by velocity) that the magnetic field in the core has to travel to get from some starting envelope or boundary value to the central value. In proper dimensionless form, this distance is $1 - f_0$. This task is accomplished at the rate $\propto \epsilon f_0^3$ on the right-hand side; therefore, when the left-hand side equals the right-hand side, we have $(1-f_0) \propto \epsilon f_0^3$. An order unity quantity on the left-hand side cannot equal an order ϵ quantity on the right-hand side unless there is a relatively large proportionality factor on the right-hand side. Although this factor might depend on f_0 (because of the specifics of the model), the dependence should be fairly slow, since the major dependences should be captured by our scaling arguments. The proportionality factor $I(f_0)/(1+2f_0^2)^{1/2}$ in equation (85) has precisely these two

qualities: (1) it is relatively large, and (2) it is relatively constant as a function of f_0. Thus, apart from minor quibbles about exactly what function $I(f_0)/(1+2f_0^2)^{1/2}$ should be, the relationship derived as equation (85) is insensitive to the details of geometry or whether ambipolar diffusion is primarily driven by pressure gradients or magnetic tension, etc.

The physics behind why it is difficult to drive the central flux-to-mass ratio f_0 to low values is now obvious. As ambipolar diffusion occurs and $|\boldsymbol{B}|$ decreases, the rate of diffusion, proportional not only to ϵ but also to $|\boldsymbol{B}|^3$, slows down appreciably. It thus becomes increasingly difficult to make $|\boldsymbol{B}|$, relative to Σ, which is the proper comparison field for $|\boldsymbol{B}|$, even smaller. As a result, many condensing cores get stuck around $f_0 \approx 0.5$ before gravitational instability takes over and the ratio $|\boldsymbol{B}|/\Sigma \propto f \propto \lambda^{-1}$ is swept into regions close to the origin for further adventures in the exciting process called star formation (Mouschovias 1976; Shu et al. 2007).

To see graphically the formal flux-to-mass profiles implied by our models, we rewrite equation (41) in the present notation as

$$f(\xi,\tau) = f(1,\tau_1) - \frac{(1-f_0)}{N_0(1)}[N_0(1) - N_0(\xi)]. \qquad (87)$$

Before runaway condensation occurs, there is not much fluid motion (if we ignore the presence of turbulence), and every region can be connected to a nearly static common envelope by characteristics from the past, so $f(1,\tau_1) = 1$. For $\xi > 1$, $N_0(\xi)$ is essentially equal to $N_0(1)$ and we have $f(\xi,\tau) = 1$, which identifies such regions as corresponding to the common envelope. For $\xi < 1$, $N_0(\xi) < N_0(1)$ according to Figure 4, and $f(\xi,\tau)$ has a value less than 1, i.e., the common envelope makes a transition to a core region undergoing ambipolar diffusion with magnetic flux leaking from the $\xi < 1$ core into the common envelope $\xi > 1$. In particular, for $\xi = 0$, $N_0(\xi) = 0$, so the central flux-to-mass value of the core is $f(0,\tau) = f_0$. The top panel of Figure 5 shows the flux profile $f(\xi) = 1 - [(1-f_0)/N_0(1)][N_0(1) - N_0(\xi)]$ before the onset of runaway condensation for the realistic cases of $f_0 = 0.75$ and 0.50. Because the function $N_0(\xi)$ is computed assuming values of $\sigma(\xi)$ and $v(\xi)$ applicable during runaway condensation (see Fig. 4), this profile should really be considered appropriate only for the specific time $\tau = 1$ demarcating the *transition* from quasi-static evolution by ambipolar diffusion to runaway core condensation.

After runaway condensation occurs, we can no longer set the advective contribution $f(1,\tau_1)$ equal to 1, because $\xi > 1$ at $\tau \ll 1$ lies in the *future* from $\xi = 1$ at $\tau_1 \sim 1$ where ambipolar diffusion has already occurred to modify f from the value of unity. Instead, $f(1,\tau_1)$ becomes the dominant *variable* term. In comparison, the *ongoing* diffusion term proportional to $\hat{\epsilon}$ becomes increasingly negligible as the difference $N_0(1) - N_0(\xi)$ vanishes, because all relevant values of ϖ correspond to $\xi = \varpi/\Theta^{1/2} a t_0 \tau > 1$. The physical meaning of this result is that approximate field freezing applies during the phases of runaway condensation followed by true gravitational collapse, and the flux-to-mass ratio plotted as a function of interior mass becomes fixed in the subsequent evolution. Only when very high densities are reached is the assumption of field freezing again violated, perhaps involving the formation of a circumstellar disk if we had included the effects of core rotation (see the discussion in § 7).

The bottom panel of Figure 5 plots the flux profile f versus the reduced and scaled enclosed mass $m(\xi)$ for the same cases depicted in top panel. This plot shows that the central value f_0 is a substantial underestimate of the average flux-to-mass ratio of the entire core, i.e., most of the core has a flux-to-mass ratio closer to unity. Correction for the underestimate should act to reduce the

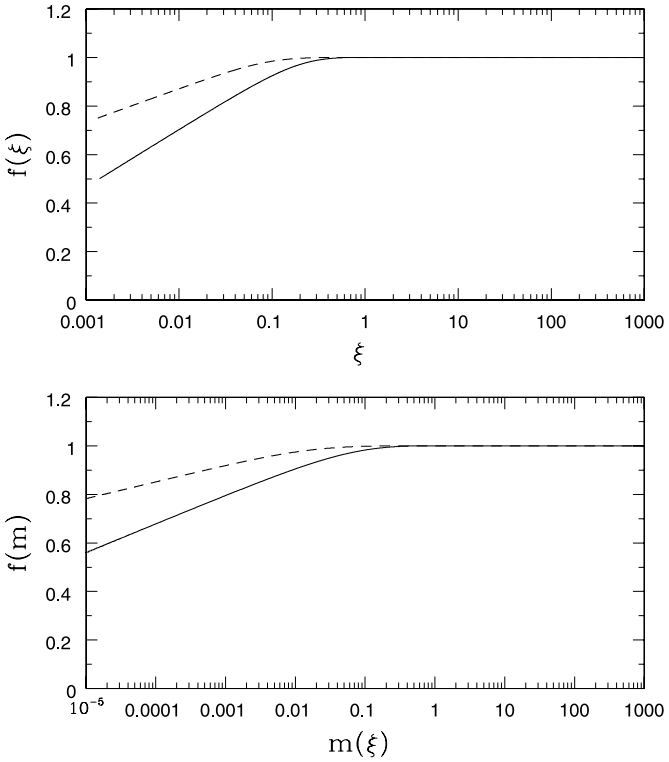

FIG. 5.—Flux-to-mass ratios. *Top*: Profiles $f(\xi)$ for $f_0 = 0.50$ (*solid curve*) and 0.75 (*dashed curve*). *Bottom*: Flux-to-mass ratio $f(m)$ as a function of enclosed mass $m(\xi)$ for the same cases, i.e., $f_0 = 0.50$ (*solid curve*) and 0.75 (*dashed curve*).

head start velocities of real molecular cloud cores in comparison with the values given in Table 1. In particular, we can expect extended contraction of the magnitude $-v_\infty$ only where and when f is still climbing to unity. Application of this rule to Figure 5 indicates that extended contraction might be observed, perhaps, to about 1/3 of the distance to the outer core boundary (about 1/3 of the enclosed core mass). As mentioned above, these estimates can be made more rigorous using singular perturbation theory with multiple length scales, where the region discussed in § 5 is treated by "intermediate asymptotics" with a scale between the large ones of the common envelope and the small ones of the runaway condensation that produces a gravomagneto catastrophe as $t \to 0^-$. Although we have not performed such an improved analysis, we hope that the naive treatment of this paper elucidates the *physical* basis of the phenomenon of gravomagneto catastrophe.

In any case, at the moment of gravomagneto catastrophe the enclosed mass in physical units inside $\varpi = \varpi_{\rm ce}$ is given by

$$M_{\rm core} = \frac{A\Theta_0 a^2}{(1-f_0^2)G}\varpi_{\rm ce} = A\left(\frac{1+2f_0^2}{1-f_0^4}\right)M_{\rm bench}, \qquad (88)$$

where the second equality uses the definition of Θ_0 and defines a benchmark mass scale $M_{\rm bench} = a^2\varpi_{\rm ce}/G$. For typical values of $a = 0.20$ km s^{-1} and $\varpi_{\rm ce} = 0.2$ pc, for example, $M_{\rm bench} \approx 1.9\ M_\odot$. The range of f_0 is limited because values of $f_0 < 0.3$ imply values of ϵ greater than unity. Over the range from 0.3 to (say) 0.9 (roughly, $1 > \epsilon > 0.002$), the core masses implied by equation (88) vary from $2.5M_{\rm bench}$ to $11M_{\rm bench}$. Note that this range in mass scale, a factor of 4.4, is smaller than the observed range of stellar masses. However, the values of a^2 and $\varpi_{\rm ce}$ that specify the mass scale $M_{\rm bench}$ can also vary, and the distribution of these parameter values will add additional width to the resulting distribution of core masses. Moreover, final stellar masses can be

appreciably smaller than the core masses at the beginning of dynamical collapse because of various inefficiencies in the actual star formation process (such as binary formation and magnetocentrifugally driven winds leading to bipolar outflows). These variations will also add width to the distribution of stellar masses (see Adams & Fatuzzo 1996 for greater mathematical detail). Taken as a whole, a strength of ambipolar diffusion as a core formation mechanism is that, given plausible variations of a^2 and ϖ_{ce}, it is capable of producing a core mass distribution wide enough, when the pivotal state is reached, to span the likely precollapse states for making brown dwarfs to high-mass stars.

6. SHEET COLLAPSE SOLUTION

The analysis presented thus far accounts for the formation of centrally condensed molecular cloud cores through the process of ambipolar diffusion. This phase corresponds to negative times ($t < 0$) and can be smoothly matched onto collapse solutions at positive times ($t > 0$). Although the collapse portion of the problem has been considered previously (e.g., Shu 1977; Hunter 1977; Galli & Shu 1993; Li & McKee 1996; Li & Shu 1997; Krasnopolsky & Königl 2002; Shu et al. 2004; Fatuzzo et al. 2004; Tassis & Mouschovias 2005; Galli et al. 2006), here we present a brief reexamination of the problem and find the particular solution that matches onto the solution to the precatastrophe problem found in §§ 4 and 5.

The equations of motion for collapse are the continuity equation (1) and the force equation (2). For simplicity, in this treatment we assume flux freezing during dynamical collapse until very small scales are reached (see Galli & Shu 1993; Galli et al. 2006; Shu et al. 2006) so that $g + \ell = (1 - f_0^2)g$. Also to keep the discussion uncomplicated and because there is now a true physical monopole (the protostar) to keep the inflowing material spatially flat, we consider the sheet monopole limit for the gravitational force (see § 4). Here the relevant similarity transformation has the form

$$x = \frac{\varpi}{at}, \quad \Sigma(\varpi, t) = \frac{a}{2\pi G t}\tilde{\sigma}(x), \quad u(\varpi, t) = a\tilde{v}(x). \tag{89}$$

After some algebra, the dimensionless self-similar form of the equations of the motion become

$$\tilde{\sigma}\frac{d\tilde{v}}{dx} + (\tilde{v} - x)\frac{d\tilde{\sigma}}{dx} = \tilde{\sigma}\frac{(x - \tilde{v})}{x}, \tag{90}$$

$$(\tilde{v} - x)\frac{d\tilde{v}}{dx} + \frac{\Theta_0}{\tilde{\sigma}}\frac{d\tilde{\sigma}}{dx} = \left(1 - f_0^2\right)\tilde{\sigma}\frac{(\tilde{v} - x)}{x}, \tag{91}$$

where Θ_0 and f_0 have the same meaning as before and are taken to be constants.

Next we apply the adopted scaling transformation

$$\xi = \frac{x}{\sqrt{\Theta_0}}, \quad v = \frac{\tilde{v}(x)}{\sqrt{\Theta_0}}, \quad \sigma = \tilde{\sigma}(x)\frac{\left(1 - f_0^2\right)}{\sqrt{\Theta_0}}. \tag{92}$$

The equations of motion then take the forms

$$\mathcal{D}\frac{dv}{d\xi} = \frac{\xi - v}{\xi}[\sigma(\xi - v) - 1], \tag{93}$$

$$\mathcal{D}\frac{d\sigma}{d\xi} = \sigma\frac{(\xi - v)}{\xi}[\sigma - (\xi - v)], \tag{94}$$

where the discriminant is now given by

$$\mathcal{D} = (\xi - v)^2 - 1. \tag{95}$$

In the outer limit $\xi \to \infty$, the equations of motion allow the asymptotic forms

$$\sigma = \frac{A}{\xi}, \quad v = v_\infty + \frac{(1 - A)}{\xi}. \tag{96}$$

In order for the collapse solution to match onto the precatastrophe solution for $t < 0$, the constants A and v_∞ must be the same as those of § 4.3. Note also that the sign of the correction term in the velocity field is different for the two cases, as it should be. The limit $\xi \to \infty$ corresponds to $t \to 0$ from either side of zero, where the solutions must match and where both solutions have velocity v_∞ (which is negative, since the core is contracting). For large but finite ξ and negative times, the condensation solution has a positive correction to the velocity, so that the velocity is smaller in magnitude, i.e., it has not reached its full head start speed that it will at the moment of gravomagneto catastrophe $t = 0$. For large but finite ξ and positive times, the collapse solution has a negative correction to the velocity, indicating that the fluid is speeding up as it collapses.

In the inner limit $\xi \to 0$, the scaled equations of motion imply that the solutions have the form of a free-fall collapse flow, i.e.,

$$\sigma = \left(\frac{m_0}{2\xi}\right)^{1/2}, \quad v = -\left(\frac{2m_0}{\xi}\right)^{1/2}, \tag{97}$$

where

$$m_0 = \lim_{\xi \to 0} m(\xi) = \text{const}. \tag{98}$$

Finding the constant m_0 is the most important result of the numerical procedure, since the rest of the solution is then specified by the similarity transformation. In particular, the dimensional mass infall rate $\dot{M}$ is given by

$$\dot{M} = \frac{a^3}{G}\tilde{m}_0 = \frac{\left(\Theta_0^{1/2}a\right)^3}{G\left(1 - f_0^2\right)}m_0. \tag{99}$$

Relative to the standard formula, the scaling of the final expression has the following mnemonic: (1) the relevant velocity to be cubed is the magnetosonic speed $\Theta_0^{1/2}a$, and (2) the relevant gravitational constant is the magnetically diluted value $(1 - f_0^2)G$.

The solution for m_0 is specified by the pair of constants (A, v_∞) that determine how the collapse solution for $t > 0$ matches onto the condensation solution for $t < 0$. Furthermore, all viable pairs of boundary values (A, v_∞) correspond to states that are overdense $(A > 1)$ and/or with finite head start velocity $-v_\infty > 0$. These solutions thus correspond to the "outer" solutions in the nomenclature of Shu (1977) or the generalization to include nonzero starting velocities (Fatuzzo et al. 2004). In any case, for these "outer" solutions the flow does not go through a critical point. As a result, one can directly integrate the equations of motion from asymptotically large ξ (where the solution matches onto those of § 5) down to small $\xi \ll 1$ to determine the constant m_0.

For the sheet monopole solution to the $t < 0$ evolution, the boundary values are $(A, v_\infty) = (1.401, -0.4952)$. Using these starting conditions, the resulting collapse solution for $t > 0$ is shown as the dashed curves in Figure 6. For this case, the inner constant $m_0 = 1.670$, about 70% larger than the coefficient found by Shu (1977) for the collapse of the critically stable, singular isothermal sphere, $m_0 = 0.975$. For the softened monopole solution to the $t < 0$ evolution, the boundary values are $(A, v_\infty) = (1.83, -0.684)$. For this case, the mass infall constant for $t > 0$ is $m_0 = 2.85$, and the resulting solution is shown as the solid curves in Figure 6.

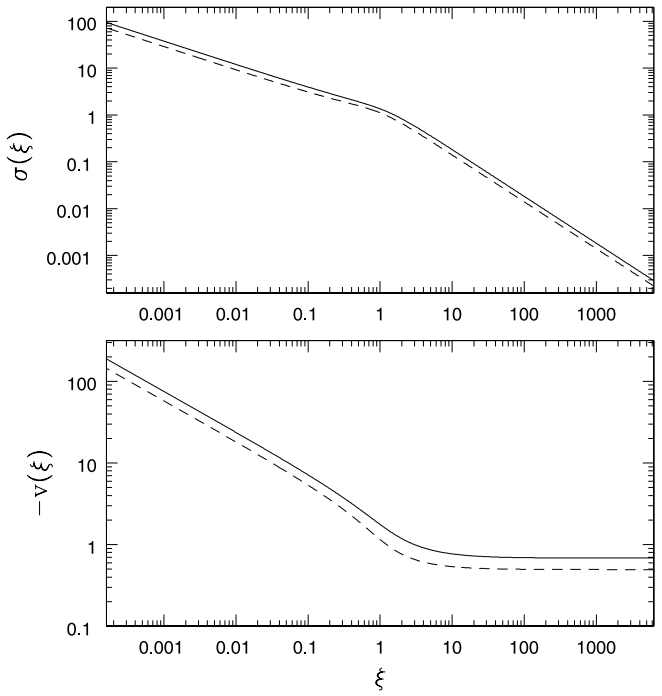

FIG. 6.—Reduced fields for collapse solution in the sheet monopole (*dashed curves*) and softened monopole (*solid curves*) approximations. *Top*: Reduced and scaled density field $\sigma(\xi)$. *Bottom*: Solution for the reduced and scaled velocity field $v(\xi)$. The initial conditions for collapse are taken to be those predicted from the condensation calculation (see Fig. 1).

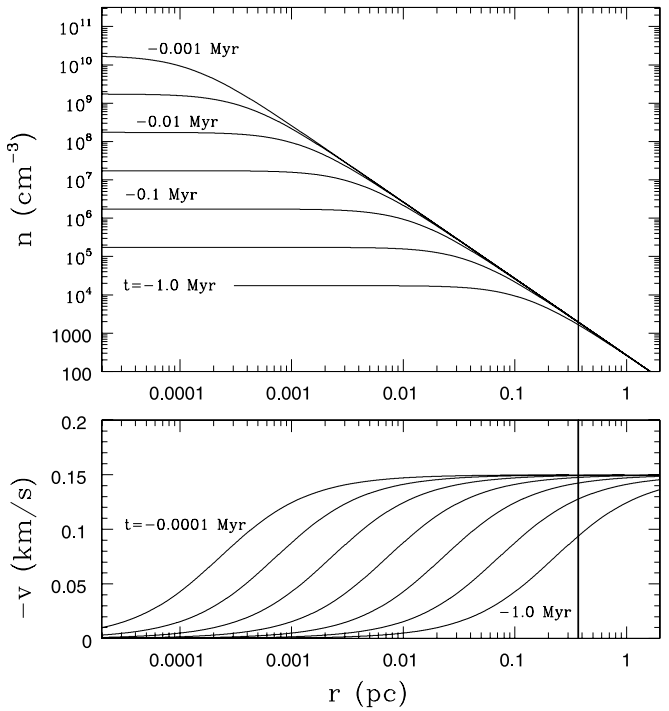

FIG. 7.—Physical solutions for the number density and velocity of a molecular cloud core during its condensation (formation) epoch for varying times before the moment of gravomagneto catastrophe (which occurs at $t = 0$). The displayed time levels are spaced logarithmically, e.g., −0.316 Myr separates the curves labeled −1.0 Myr and −0.1 Myr in the top panel. The vertical solid lines mark the location of the outer core boundary, if it were set by the condition that the density falls to a benchmark value $n = 1000$ cm^{-3}, where a core would join onto the background molecular cloud. The displayed velocity field is probably not trustworthy when one has reached about 1/3 of the distance to the outer core boundary.

We note that the collapse solution presented here is somewhat idealized, even within the class of possible self-similar solutions. The collapse flows shown in Figure 6 are calculated from the sheet monopole and softened monopole approximations for the gravitational field. For cases that include a full calculation of the perturbational gravity and no initial inward velocities (e.g., Li & Shu 1997; Krasnopolsky & Königl 2002), a shock front develops just outside the infall region. Except for the region near the shock, which includes the transition between the inner collapsing flow and the outer quasi-static region, the solutions with and without shocks are qualitatively and quantitatively similar. Specifically, the collapse solutions with monopole gravity (and no shock front) result in a reduced point mass $m_0 \approx 1.3$, whereas the case of full gravity solutions (with a shock front) result in $m_0 \approx 1.05$ (Li & Shu 1997). In the case considered here, however, the $t = 0$ configurations (at the end of the ambipolar condensation phase and the start of the collapse phase) have nonzero inward velocities which act to eliminate the critical points in the flow (e.g., Fatuzzo et al. 2004), so that we do not expect shocks near the head of the expansion wave to play a significant role in the collapse.

This treatment also neglects the effects of rotation on collapse. The solutions found here thus represent the outer portion of the collapse flow and must be matched onto inner solutions that include rotation (Cassen & Moosman 1981; Terebey et al. 1984). When the inner portion of the outer region approaches ballistic (pressure-free) conditions, this matching can be done seamlessly (Shu 1977; Li & Shu 1997; Fatuzzo et al. 2004). For collapse flows that include magnetic fields, however, the roles of magnetic braking and magnetorotational instability (MRI) can be important (see Allen et al. 2003; Galli et al. 2006; Shu et al. 2006, 2007). The calculations of this paper show that if field freezing strictly holds for the collapse phase $t > 0$, then the value of λ_0 brought into the star plus disk would be typically ~ 2, which could prevent disk formation by magnetic braking; this result has also been found in numerical simulations (e.g., Fromang et al. 2006; Price & Bate 2007). How circumstellar disks form and evolve thus remains an open question, although it appears likely that global MRI in a context of nonzero net flux will play a major role (Shu et al. 2007).

7. ILLUSTRATIVE NUMERICAL EXAMPLE

To give astronomical context to the semianalytic results of this paper, we next plot the evolution given by the softened monopole condensation and collapse solutions in dimensional form for the case $f_0 = 0.5$ and $a = 0.2$ km s^{-1}. In Figures 7 and 8 we show the equatorial volume density $\rho(\varpi, 0, t) \equiv \Sigma/2z_0$, plotted here as the number density $n = \rho/2.3m_{\rm H}$, and the equatorial inflow velocity $-u(\varpi, t)$ as functions of ϖ and t. Figure 7 shows the time evolution for negative times $t < 0$ (starting from $t = -1.0$ Myr), whereas Figure 8 shows the time evolution for positive times $t > 0$ (out to $t = +1.0$ Myr). Note that the evolution of the runaway condensation phase for $t < 0$, as shown by Figure 7, compares well with the calculations of ambipolar diffusion carried out numerically by Basu & Mouschovias (1994).

The important thing to carry away from Figure 7 is that condensing cores are not observable in dense gas tracers such as NH_3, which requires $n > 3 \times 10^4$ cm^{-3} for excitation, until the cores are within several hundred thousand years of gravomagneto catastrophe. If "cores" are defined as such by whether they are observable in dense gas tracers, then their "lifetimes" will be comparable to the lifetimes of embedded protostars, also measured in the several hundreds of thousands of years. This numerical coincidence results in roughly equal numbers for "starless cores" and "cores with embedded stars," with considerable scatter depending on the

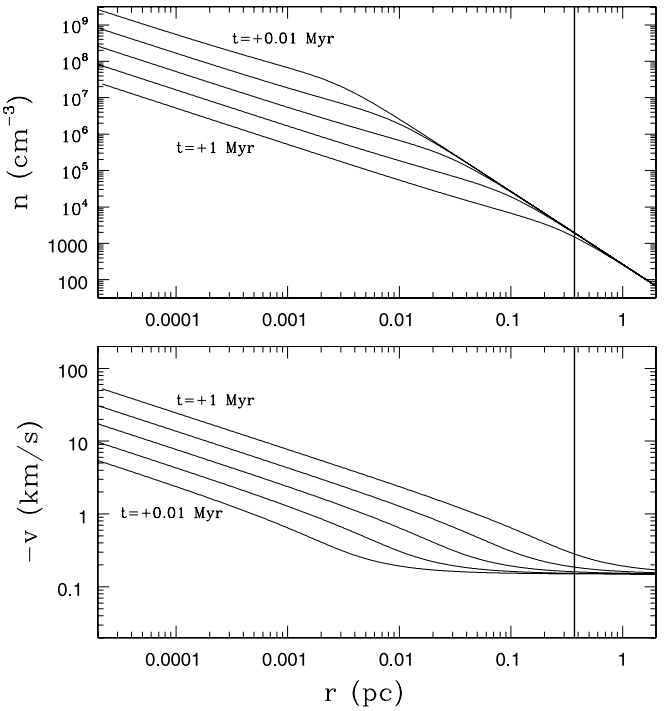

FIG. 8.—Physical solutions for the number density and velocity of a molecular cloud core during its collapse epoch for varying times $t > 0$ after the moment of catastrophe. The five curves in each panel correspond to logarithmically spaced time intervals, i.e., the times +0.0316 Myr, +0.1 Myr, and +0.316 Myr lie between the displayed times of +0.01 Myr and +1 Myr. The vertical solid lines mark the location of the outer core boundary, if it were set by the condition that the density falls to a benchmark value of $n = 1000$ cm^{-3}, where a core would join onto the background molecular cloud. The displayed region of extended infall is probably not trustworthy when one has reached about 1/3 of the distance to the outer core boundary.

value of ϵ in the region being studied. Similar statistics given by observers, plus the finding that the surface density profiles of cores are flat in their central parts, have led to the mistaken criticism that ambipolar diffusion seems to work too slowly to account for the observations (e.g., André et al. 1996; Ward-Thompson et al. 1999). Runaway core condensation, the phase depicted in Figure 7, does not take long, but it is just the last stage of the ambipolar diffusion process. Indeed, it is a stage where not much ambipolar diffusion is still going on, with the central flux-to-mass f_0 being "frozen" in value. Prior to this stage, there were slower stages of evolution, lasting maybe an order of magnitude longer than 10^6 yr (although it is hard to specify when to start the clock for this less definite problem), where ambipolar diffusion *did work* to get the central regions into the runaway state (see Fig. 5). These stages are not well studied by the similarity methods of this paper, but have been amply treated by many numerical simulations (e.g., Nakano 1979; Lizano & Shu 1989; Basu & Mouschovias 1994; Desch & Mouschovias 2001), and they occupy the bulk of the evolution time starting from arbitrarily chosen "initial" conditions.

The fact that the inflow velocities of "extended contraction" are observed to be a significant fraction of the sound speed a indicates that once runaway condensation commences, the process is fairly rapid. Nevertheless, if the extended inflow velocities typically reach half the magnetosonic speed, the core is roughly within 75% of being "magnetohydrostatic." As a result, the oft-repeated statement that "star formation is a dynamical process" is an illusion when applied to $t < 0$, and it is a tautology when applied to $t > 0$. Observations of extended converging flows thus do not support the view of star formation as a turbulent dynamic process, nor do they refute the theory of ambipolar diffusion as the core formation mechanism. Indeed, as we argue in § 8, the magnitude of the observed inflow velocity is fully consistent with the predictions of this paper and thus provides a strong argument that molecular cloud core formation, at least in isolated regions of relatively low total mass, is due to ambipolar diffusion.

For the collapse phase ($t > 0$), Figure 8 shows that the fluid fields display the usual forms, as studied in many previous treatments (e.g., Shu 1977; Hunter 1977; Galli & Shu 1993; Allen et al. 2003; Fatuzzo et al. 2004). In particular, as the collapse proceeds, the densities at a given radius ϖ become increasingly *smaller* than in the pivotal state before it. This behavior is a consequence of the solution belonging to the family of *expansion-wave* collapse solutions (Shu 1977), with the material missing from the inner core collecting in a pointlike object (the forming star) at the center of the collapse flow. In the new case considered here, the collapse solution at positive times matches smoothly onto the condensation solution of negative times. Not only does this generalization provide a self-contained picture of core formation and subsequent collapse, but it also shows that the starting state for collapse has a nonzero inward velocity, which results in a somewhat larger mass infall rate. The trend of decreasing density at a given radius ϖ is thus more extensive than in the case of a magnetohydrostatic starting state, because the "piston" is pulled in by the head start velocities more rapidly and in a more continuous manner.

8. DISCUSSION AND CONCLUDING REMARKS

In this paper, we have presented a picture of molecular cloud core formation that envisages a process of the slow leakage of magnetic flux from a dense pocket of gas and dust via ambipolar diffusion. This process continues until the central regions acquire a mass-to-flux ratio $\lambda_0 = f_0^{-1}$ that is too high for continued quasi-hydrostatic support against the self-gravity of the core, and the core develops a runaway central density with a power-law profile $\Sigma \propto \varpi^{-1}$ or $\rho \propto r^{-2}$ at the moment of gravomagneto catastrophe $t = 0$. One of the key findings of this paper is that f_0 is given by the root of equation (85),

$$\frac{(1 - f_0)}{f_0^3 K(f_0)} = \epsilon, \tag{100}$$

where $K(f_0) \equiv I(f_0)/\left(1 + 2f_0^2\right)^{1/2} \sim 25$ for values of f_0 of physical interest, and ϵ is the dimensionless rate of ambipolar diffusion given by equation (20). This equation shows that it is difficult for ambipolar diffusion to produce regions with $f_0 < 0.3$ without an anomalously high effective rate coefficient $\epsilon > 1$. A more typical outcome is probably $f_0 \sim 0.5$, although values of f_0 close to unity might be sustainable in regions with high ionization rates (which lowers ϵ). Such regions will be characterized by high surface densities $\Sigma \propto (1 - f_0^2)^{-1}$, and therefore large visual extinctions, as well as large core masses, and could be one ingredient to the cores that make massive stars. Another ingredient could be high gas temperatures or high levels of turbulence.

During the epoch of core formation, $t < 0$, extended regions of contraction develop and extend to perhaps one-third of the way to the effective boundary where the core joins onto a common envelope of the dense clump that surrounds it (see § 5.3 and Fig. 5). Significantly, the contraction velocities are always beneath the magnetosonic value. A transition to fully dynamic flow is made for $t > 0$ that corresponds to an inside-out collapse solution, but with a submagnetosonic head start velocity and an overdense outer envelope given to the region by the ambipolar diffusion process in the previous epoch $t < 0$. The main feature of the $t > 0$ collapse solution is self-similar infall onto a growing protostar at a mass infall rate $m_0(\Theta_0^{1/2} a)^3/(1 - f_0^2)G$, where the

dimensionless coefficient m_0 is 2 or 3 times larger than the "standard" value of 0.975 (resulting from purely hydrostatic states at $t = 0$). In some sense, this new solution combines the most attractive features of the self-similar solutions proposed in previous work (e.g., Larson 1969; Penston 1969; Shu 1977; Hunter 1977; Fatuzzo et al. 2004) without bearing any of the unnecessary baggage.

The models predict that the head start velocities are correlated with overdensities. Compared to the static singular isothermal sphere (SIS), the submagnetosonically inflowing parts of the core characterized by r^{-2} volume densities have total overdensity factors of $A(1 + 2f_0^2)/(1 - f_0^4)$. For $f_0 = 0.5$ in the softened monopole model where $A = 1.83$ (see Table 1), this amounts to an overall factor of 3. From a near-infrared extinction study of the bipolar outflow source B335, Harvey et al. (2001) found the outer portions of its associated core to have a r^{-2} power-law behavior for the inferred volume density, with an overdensity relative to the SIS of 3–5. They interpreted their data in terms of an unstable Bonnor-Ebert sphere. Later, Harvey et al. (2003b) found the inner portions of B335 to have a density profile consistent with a $r^{-3/2}$ law, i.e., consistent with the detailed modeling of this source as a classic example of inside-out collapse (Zhou et al. 1993; Choi et al. 1995; Evans et al. 2005). In a study of the starless globule L694-2, which has strong evidence for inward motions, Harvey et al. (2003a) find the outer portion of the core to have a $r^{-2.6}$ volume density profile, steeper than our model predictions, but with an overdensity factor in its central regions relative to Bonnor-Ebert extrapolations of about 4. While these authors speculate that the effect might arise from the core being a prolate object viewed along its long axis, a more satisfying and unified interpretation is that B335 is a $t > 0$ postcatastrophe core with an embedded protostar (and bipolar outflow), magnetized at $f_0 \approx 0.5$; and that L694-2 is a $t < 0$ precatastrophe starless core, magnetized also at $f_0 \approx 0.5$. Another indicator of the correctness of this identification is that the predicted mass infall rate $\dot{M} = m_0(\Theta_0^{1/2}a)^3/(1 - f_0^2)G$ is roughly consistent with measured values in Class 0 sources (for examples with estimates at the extremes, see Ohashi et al. 1997; Furuyu et al. 2006), despite earlier claims that Class 0 protostars would have much higher infall rates (e.g., Henriksen et al. 1997).

The (near) self-similarity of the problem is a particularly attractive feature of the process. Given that the central portions of the core are nearly isopedic, i.e., that $\lambda = 1/f$ is nearly a spatial constant, self-similarity of the collapse solution for $t > 0$ (but not too much greater) or even for the runaway core condensation phase for $t < 0$ (but not too much less) is perhaps not a surprising outcome of nature's tendency to produce power laws when solutions have to span large dynamic ranges in space and time.

However, the reader could rightfully question whether the f-profiles obtained in Figure 5 are not special to the application of self-similarity to a problem—the initial stages of the condensation of a cloud core by ambipolar diffusion—that has no good reason, beyond mathematical convenience, to be self-similar. After all, the contraction of typical molecular densities in clumps of $\sim 10^3$ cm^{-3} to early-stage cloud cores with number densities $\sim 3 \times 10^4$ cm^{-3} can hardly be characterized as spanning a very large range. One might think that the resulting f-profiles would show considerable variation depending on the exact initial state being assumed and boundary conditions being applied. And so it must be with very detailed descriptions of such early stages of cloud evolution. But if one is pressed for more global trends, there are only so many ways that a function f can monotonically go from unity at some large radius to some other value f_0, typically 1/2, at some small radius. And a self-similar approach to getting such a profile is probably not any worse than some other ad hoc prescription. The important features of the picture are not the details of the f-profiles, but the global view provided by estimates of the relevant timescales, relationships between ϵ and f_0, generic stages of the evolution, and the final asymptotic convergence to self-similarity as the moment of gravomagneto catastrophe is approached and passed.

In particular, the solutions presented in this paper are compatible with full ambipolar-diffusion calculations that start with marginally subcritical configurations which develop nearly isopedic central cores (with $\lambda \approx$ const) before proceeding on a path of extended gravitational condensation that leads to gravomagneto catastrophe (Nakano 1979; Lizano & Shu 1989; Basu & Mouschovias 1994). It is particularly significant that both the predicted and observed contraction velocities are submagnetosonic and arise from the modest overdensities that are left behind in the contracting cores as their magnetic support leaks to the common envelope. Thus, the observed head start velocities are an indicator that some slow process like ambipolar diffusion is at work producing molecular cloud cores, rather than some more sudden process of the destruction of high levels of nonthermal support, such as the dissipation of hypersonic turbulence through shock waves. The latter description may still apply, however, in the crowded conditions that characterize high-mass star-forming regions.

The most important lesson of this paper is that the details of the ambipolar diffusion process control only the spatial extent of the region of extended, submagnetosonic contraction and the timing of the runaway core condensation that leads to the gravomagneto catastrophe. Provided the small parameter ϵ is not strictly zero, gravomagneto catastrophe is the unavoidable fate of a lightly ionized, isolated molecular cloud core, as long as Lorentz forces contribute to the support against its self-gravitation (see the discussion of Lizano & Shu 1989 concerning "failed cores"). Given that the inner cores acquire nearly isopedic states with $\lambda = 1/f \approx$ const, the resulting density and magnetic field profiles of the resulting runaway condensation steepen into generic power laws and are robust.

This work was initiated during a sabbatical visit of F. C. A. to UCSD; we would like to thank the Physics Departments at both the University of Michigan and the University of California, San Diego, for making this collaboration possible. Discussions with Mike Cai were very helpful. This work was supported through the University of Michigan by the Michigan Center for Theoretical Physics; by NASA through the Astrophysics Theory Program (NNG 04-GK56G0) and the *Spitzer Space Telescope* Theoretical Research Program (1290776).

APPENDIX A

MAGNETIC FORCES IN A THIN DISK

In this appendix, spurred by a correction pointed out by M. Cai (2007, private communication), we revisit the derivation given by Shu & Li (1997) for the magnetic forces in a thin disk. The Lorentz force per unit volume with only axisymmetric poloidal fields is given by

$$\frac{1}{4\pi}(\nabla \times \boldsymbol{B}) \times \boldsymbol{B} = \frac{1}{4\pi}\left(\frac{\partial B_z}{\partial \varpi} - \frac{\partial B_\varpi}{\partial z}\right)(B_z \hat{\boldsymbol{e}}_\varpi - B_\varpi \hat{\boldsymbol{e}}_z). \tag{A1}$$

If we integrate over z in a thin disk of effective thickness $2z_0 \ll \varpi$ with $B_\varpi^+ = -B_\varpi^-$ being, respectively, the radial magnetic field at the upper and lower surface of the disk and with B_z being continuous across the midplane, the force per unit area in the radial direction is given by

$$-\frac{B_z B_\varpi^+}{2\pi} - \frac{\partial}{\partial \varpi}\left(\frac{B_z^2 z_0}{4\pi}\right). \tag{A2}$$

We recognize the first term as what Shu & Li refer to as the force per unit area due to magnetic tension, but the second term is only the negative radial gradient of the vertically integrated magnetic pressure due to $B_z^2/8\pi$ and not $(B_z^2 + B_\varpi^2)/8\pi$. The reason is that the so-called magnetic-tension term also contains a small piece of the magnetic pressure, in fact, exactly the integral of $B_\varpi^2/8\pi$ over the disk thickness. Nevertheless, for simplicity we continue to refer to the two terms as "magnetic tension" and "magnetic pressure."

Vertical hydrostatic equilibrium for a magnetized isothermal gas in its own vertical gravitational field requires

$$-\rho\frac{\partial U}{\partial z} - a^2\frac{\partial \rho}{\partial z} - \frac{\partial}{\partial z}\left(\frac{B_\varpi^2}{8\pi}\right) = 0, \tag{A3}$$

where the last term is the dominant term for the magnetic force per unit volume in the z-direction according to equation (A1). In the above, U is the self-gravitational potential of the gas and satisfies the local Poisson's equation,

$$\frac{\partial^2 U}{\partial z^2} = 4\pi G\rho. \tag{A4}$$

The substitution of the above into equation (A3) allows us to integrate once,

$$\frac{1}{8\pi G}\left(\frac{\partial U}{\partial z}\right)^2 + a^2\rho + \frac{B_\varpi^2}{8\pi} = C(\varpi), \tag{A5}$$

where $C(\varpi)$ is a constant for fixed ϖ (and diffusion time). We evaluate C at the upper disk surface where $\partial U/\partial z = 2\pi G\Sigma$, $\rho = 0$, and $B_\varpi = B_\varpi^+$; and we do the same at the disk midplane where $\partial U/\partial z = 0$, $\rho \equiv \Sigma/2z_0$ (being a definition of z_0), and $B_\varpi = 0$. Setting equal the two expressions for the "constant" total pressure, we obtain

$$\frac{a^2\Sigma}{2z_0} = \frac{\pi G\Sigma^2}{2} + \frac{(B_\varpi^+)^2}{8\pi}. \tag{A6}$$

For an isopedic singular isothermal disk, which is what the inner parts of molecular cloud cores become at the moment of gravomagneto catastrophe,

$$B_\varpi^+ = B_z = \frac{2\pi G^{1/2}\Sigma}{\lambda}, \tag{A7}$$

with λ equal to a constant. Equation (A5) now becomes the second relation of equation (8). In the same limit, we have

$$\frac{B_z^2 z_0}{4\pi} = \left(\frac{a^2\Sigma}{1+\lambda^2}\right),$$

which shows that the sum of gas pressure force in the radial direction with the second term in equation (A1) equals $-a^2\partial(\Theta\Sigma)/\partial\varpi$ with Θ given by the first relation of equation (8) rather than by the expression $\Theta = (3+\lambda^2)/(1+\lambda^2)$ from the analysis of Shu & Li (1997). The difference (2 vs. 3 in the sum of the numerator) arises because the latter authors mistakenly included the contribution of $(B_\varpi^+)^2/8\pi$ into the computation of the magnetic "pressure" force, which duplicates a small piece already included in the first term of equation (A1).

For later reference, we consider the vertical structure if we make the assumption that the current density is proportional to the volume density, i.e.,

$$\frac{\partial B_\varpi}{\partial z} = B_\varpi^+\frac{2\rho}{\Sigma}. \tag{A8}$$

The substitution of equation (A8) into equation (A5) yields a differential equation which we may write as

$$\frac{1}{8\pi G}\left(\frac{\partial U}{\partial z}\right)^2 + \frac{a^2\Sigma}{2B_\varpi^+}\frac{\partial B_\varpi}{\partial z} + \frac{B_\varpi^2}{8\pi} = \frac{\pi}{2}G\Sigma^2 + \frac{(B_\varpi^+)^2}{8\pi}. \tag{A9}$$

The solutions for equations (A4), (A8), and (A9) read

$$B_\varpi = B_\varpi^+\tanh(z/z_0), \qquad \rho = \Sigma/(2z_0)\mathrm{sech}^2(z/z_0), \qquad -\partial U/\partial z = -2\pi G\Sigma\tanh(z/z_0), \tag{A10}$$

if we set $B_\varpi^+ = B_z = 2\pi G^{1/2}\Sigma/\lambda$. Equation (A10) represents the isopedically magnetized version of the solution from Camm (1950) and Spitzer (1955) for the stratified isothermal disk. We note in passing, however, that while equation (A7) is an acceptable approximation

in the disk proper, it must fail on the z-axis where $B_{\varpi}^{+} = 0$ from symmetry considerations, but B_z is not only nonzero but also achieves a maximum value there.

APPENDIX B

DERIVATION OF THE DIFFUSION CONSTANT

In this appendix, we present a brief discussion of the derivation of the diffusion coefficient in the magnetic diffusion equation. We start with the z-component of the induction equation including ambipolar diffusion,

$$\frac{\partial B_z}{\partial t} + \frac{1}{\varpi}\frac{\partial}{\partial \varpi}(\varpi B u) = \frac{1}{\varpi}\frac{\partial}{\partial \varpi}\left(\frac{\varpi B_z^2}{4\pi\gamma\rho\rho_i}\frac{\partial B_{\varpi}}{\partial z}\right), \tag{B1}$$

where we have kept only the largest term on the right-hand side for a highly flattened core. Here, B_z is the z-component of the field, and B_{ϖ} denotes the ϖ-component. After multiplying the equation by ρ and integrating over z, we obtain the form

$$\Sigma\left[\frac{\partial B_z}{\partial t} + \frac{1}{\varpi}\frac{\partial}{\partial \varpi}(\varpi B_z u)\right] = \frac{1}{\varpi}\frac{\partial}{\partial \varpi}\left(\frac{\varpi B_z^2}{4\pi\gamma}\int_{-\infty}^{\infty}\frac{dz}{\rho_i}\frac{\partial B_{\varpi}}{\partial z}\right) = \frac{1}{\varpi}\frac{\partial}{\partial \varpi}\left[\frac{\varpi B_z^2 B_{\varpi}^{+}(2z_0)^{1/2}}{2\pi\gamma\mathcal{C}\Sigma^{1/2}}\right], \tag{B2}$$

where we have defined

$$\frac{1}{\mathcal{C}} \equiv \frac{\Sigma^{1/2}}{(2z_0)^{1/2}B_{\varpi}^{+}}\int_0^{\infty}\frac{dz}{\rho_i}\frac{\partial B_{\varpi}}{\partial z} = \int_0^{\infty}\frac{\mathrm{sech}(z/z_0)}{\mathcal{C}_{\mathrm{local}}}\frac{dz}{z_0}, \tag{B3}$$

if we assume equation (A10) to hold and express the ion abundance by the local relation $\rho_i = \mathcal{C}_{\mathrm{local}}\rho^{1/2}$ (Shu 1992). In the present application, $\mathcal{C}_{\mathrm{local}}$ is a constant if cosmic rays provide the dominant source of ionization, but it quickly climbs to much larger values near the surfaces of molecular clouds because of the ultraviolet ionization of elements like carbon (McKee 1989). For $\mathcal{C}_{\mathrm{local}} = \mathrm{const}$, we have $\mathcal{C} = (2/\pi)\mathcal{C}_{\mathrm{local}} = 2.0 \times 10^{-16}\ \mathrm{cm}^{-3/2}\ \mathrm{g}^{1/2}$ (Shu 1992).

APPENDIX C

THE VELOCITY FUNCTION IS MONOTONIC

In this appendix, we argue that the reduced and scaled velocity field v is a monotonic function of ξ for the regime of interest. Since $v = 0$ at $\xi = 0$ (the inner boundary condition), the monotonicity of v implies that the solution must have a nonzero velocity at large ξ. In physical terms, this finding implies that starless cores are predicted to have nonzero velocities, even before the collapse phase begins (as observed). Of course, the numerical integration of the equations of motion implies nonzero values of v_{∞}. In this appendix, however, we analytically show that this property must always hold.

In order to prove this assertion, at least in the context of the approximations of this paper, it is sufficient to show that the right-hand side of equation (58) is never equal to zero except at the critical point ξ_* (where the discriminant $\mathcal{D}$ changes sign). First, we define the ancillary function

$$P(\xi) \equiv \sigma(\xi + v). \tag{C1}$$

The right-hand side of equation (58) will be zero if and only if $P(\xi) = 1$. Further, we know that $P(\xi) = 1$ at the critical point. Next we show that $P(\xi)$ is monotonic. Differentiating P with respect to ξ, we obtain

$$\frac{dP}{d\xi} = (\xi + v)\frac{d\sigma}{d\xi} + \sigma\left(1 + \frac{dv}{d\xi}\right). \tag{C2}$$

Using the equations of motion (eqs. [59] and [58]), this result simplifies to the form

$$\frac{dP}{d\xi} = \frac{-\sigma v}{\xi}. \tag{C3}$$

Since the density σ and the coordinate ξ are always positive and since we are interested in contracting solutions where v is negative, the right-hand side of this equation, and hence $dP/d\xi$, is positive. As a result, the function $P(\xi)$ is a monotonically increasing function of the variable ξ.

Since $P(\xi_*) = 1$ and $P(\xi)$ is monotonic, it follows that $P < 1$ for all $\xi < \xi_*$ and $P > 1$ for all $\xi > \xi_*$. It then follows that the right-hand side of equation (58) is positive for $\xi < \xi_*$ and negative for $\xi > \xi_*$. Since the discriminant has the opposite behavior, $\mathcal{D} < 0$ for $\xi < \xi_*$ and $\mathcal{D} > 0$ for $\xi > \xi_*$, it follows that $-dv/d\xi > 0$ for all values of ξ. Thus, v is a monotonic function of ξ, as claimed.

APPENDIX D

GENERALIZED APPROACH TO CROSSING CRITICAL LINES

In this appendix, we record the procedure needed to solve the posed problem when the force integral from equation (34) has a general form written as

$$F \equiv -\Lambda(\xi)\frac{m(\xi)}{\xi^2} = -\Lambda(\xi)\frac{(\xi+v)2\sigma}{\xi}. \tag{D1}$$

The first equality is true by definition, i.e., we define the function $\Lambda(\xi)$ to be the ratio of the true force to that given by the monopole approximation. The second equality follows from the continuity equation. The monopole approximation corresponds to the simplest case $\Lambda(\xi) = 1$.

With the introduction of the correction function $\Lambda(\xi)$, we can find the values of the fluid fields and their derivatives at the critical points. Specifically, for critical point ξ_*, we find

$$\sigma(\xi_*) = \frac{1}{\Lambda(\xi_*)}, \qquad v(\xi_*) = 1 - \xi_*. \tag{D2}$$

Using the same expansion around the critical point as before (see eq. [61]), we find the derivatives of the fluid fields at the critical point, i.e.,

$$v_1 = -\frac{1}{2} \pm \frac{1}{2\xi_*}\left[(\xi_* - 1)^2 + 1 - 2\xi_*\frac{\Lambda_*'}{\Lambda_*}\right]^{1/2}, \tag{D3}$$

$$\sigma_1 = \frac{1}{2\xi_*\Lambda_*}\left\{\xi_* - 2 + 2\xi_*\frac{\Lambda_*'}{\Lambda_*} \mp \left[(\xi_* - 1)^2 + 1 - 2\xi_*\frac{\Lambda_*'}{\Lambda_*}\right]^{1/2}\right\}. \tag{D4}$$

In these expressions, $\Lambda_* = \Lambda(\xi_*)$ and $\Lambda_*' = d\Lambda/d\xi(\xi_*)$.

APPENDIX E

MULTIPOLE APPROACH TO EFFECTIVE SHEET GRAVITY

In this appendix, we consider the multipole approach to the evaluation of the force equation (34) (see, e.g., Li & Shu 1997), which we write as

$$F(\xi) = -\frac{dU}{d\xi}, \qquad \text{where} \qquad U(\xi) \equiv \int_0^\infty \mathcal{H}_0(\xi,\eta)\sigma(\eta)\eta\, d\eta, \tag{E1}$$

with $\mathcal{H}_0$ being the classical Poisson kernel for a self-gravitating axisymmetric sheet,

$$\mathcal{H}_0(\xi,\eta) \equiv -\frac{1}{2\pi}\oint \frac{d\varphi}{\sqrt{\xi^2+\eta^2-2\xi\eta\cos\varphi}}. \tag{E2}$$

We now use the well-known formula for the spectral expansion of the inverse separation distance between a field point at ξ and a source point at η separated by an angle φ (see, e.g., eq. [3.41] of Jackson 1962),

$$\left(\xi^2+\eta^2-2\xi\eta\cos\varphi\right)^{-1/2} = \sum_{\ell=0}^{\infty}\frac{\eta^\ell}{\xi^{\ell+1}}P_\ell(\cos\varphi) \qquad \text{for} \qquad \eta < \xi, \tag{E3a}$$

$$\left(\xi^2+\eta^2-2\xi\eta\cos\varphi\right)^{-1/2} = \sum_{\ell=0}^{\infty}\frac{\xi^\ell}{\eta^{\ell+1}}P_\ell(\cos\varphi) \qquad \text{for} \qquad \xi < \eta, \tag{E3b}$$

where $P_\ell(\mu)$ are the Legendre polynomials of order ℓ.

For an axisymmetric surface density distribution $\sigma(\eta)$, we now have

$$U(\xi) = -\sum_{\ell=0}^{\infty} c_{2\ell}\left[U_{2\ell}^{<}(\xi)\xi^{-(2\ell+1)} + U_{2\ell}^{>}(\xi)\xi^{2\ell}\right], \qquad \text{where} \qquad c_{2\ell} \equiv \frac{1}{2\pi}\oint P_{2\ell}(\cos\varphi)\, d\varphi, \tag{E4a}$$

$$U_{2\ell}^{<} \equiv \int_0^\xi \eta^{2\ell}\sigma(\eta)\eta\, d\eta, \qquad U_{2\ell}^{>} \equiv \int_\xi^\infty \eta^{-(2\ell+1)}\sigma(\eta)\eta\, d\eta. \tag{E4b}$$

Our sum extends over only even values of ℓ because the coefficients c_ℓ vanish for odd ℓ. The numerical values of $c_{2\ell}$ are all positive; according to (an equivalent formula by) Gradshteyn & Ryzhik (1980, eq. [7.222]),

$$c_{2\ell} = \left[\frac{(2\ell-1)!!}{(2\ell)!!}\right]^2.$$

Thus, $c_{2\ell} = 1, 1/4, 9/64, 25/256, 1225/16,384, 3669/65,536$, etc., for $2\ell = 0, 2, 4, 6, 8, 10$, etc., declining slowly only as $\sim 1/2\ell$ for large ℓ. We refer to $U_{2\ell}^<$ and $U_{2\ell}^>$ as, respectively, the interior (or inner) and the exterior (or outer) multipole moment of order 2ℓ with $2\ell = 0, 2$, etc., corresponding to the monopole, quadrupole, etc. In any case, if we now carry out the differentiation indicated in equation (E1), we get

$$F(\xi) = \sum_{\ell=0}^{\infty} c_{2\ell}\left[-(2\ell+1)U_{2\ell}^<(\xi)\xi^{-(2\ell+2)} + 2\ell U_{2\ell}^>(\xi)\xi^{2\ell-1}\right], \tag{E5}$$

where we have used the fact that each multipole order cancels in pairs if we differentiate the moments rather than the powers of ξ. Note that only the interior monopole moment term $\propto U_0^<$ survives this differentiation because $2\ell U_{2\ell}^>$ equals zero when $\ell = 0$. This well-known result is fortunate, since $U_0^>$ is formally logarithmically divergent if $\sigma(\eta) \to A/\eta$ at large η.

If $\sigma(\eta) = A/\eta$ for all η from 0 to ∞, then $U_{2\ell}^< = \xi^{2\ell+1}/(\ell+1)$ and $U_{2\ell}^> = \xi^{-2\ell}/2\ell$ (except for $\ell = 0$), and all multipoles cancel in pairs in F except for $\ell = 0$. As is well-known, the radial force field for a perfect singular isothermal disk (SID) is given solely by the interior monopole. When $\sigma(\eta)$ departs from the ideal SID state, say, by becoming a constant σ_0 in the central regions, then $U_{2\ell}^< \approx \sigma_0\xi^{2\ell+2}/(2\ell+2)$ for small ξ, so each interior multipole contributes a constant term to $F(\xi)$ at small ξ. But the exterior multipole moments will now contribute terms that are larger, and opposite in sign, to their interior multipole counterparts. Thus, the effect of including multipoles *reduces* the inward force of $F(\xi)$ at small ξ relative to the monopole contribution for given A.

Computing $F(\xi)$ by equation (74) is equivalent to summing the infinite set of multipole contributions. In either case, we can compute the correction function $\Lambda(\xi)$ of Appendix D as

$$\Lambda(\xi) = \frac{-F\xi^2}{m}, \tag{E6}$$

where $m \equiv U_0^<$. If the correction function $\Lambda(\xi)$ were known, then one could find the solution using the same procedure as before (in § 4 for the monopole solution): guess the value of the critical point, move inward from the working estimate of ξ_* using the results of § 4.2, and integrate inward to the origin. Then adjust the value of the critical point and iterate until the inner boundary conditions are satisfied. After finding the critical point, one further integration of the equations of motion (both inward to the origin and outward to large ξ) then determines the solution. In this case, however, we do not know the function $\Lambda(\xi)$, and its form depends on the solution for $\sigma(\xi)$ that we are trying to find. As a result, we must use another iterative scheme. We first estimate (guess) the form of the function $\Lambda(\xi)$ and then calculate the (approximate) solution according to the previous procedure. With this approximation to σ, we can evaluate the integrals in equations (E4a) and (E4b) to find a new estimate for the correction function $\Lambda(\xi)$. We then iterate this procedure until the solution is obtained.

APPENDIX F

FULL EFFECTIVE GRAVITY OF UNFLATTENED CORE

In this appendix, we consider the properties of the full gravity of an incompletely flattened core. This can be carried out by replacing the kernel $\mathcal{H}_0(\xi,\eta)$ by the weighted average of the product of the volume densities at the source and field points of the three-dimensional Poisson integral (see eq. [A9]),

$$\mathcal{H}(\xi,\eta) \equiv -\frac{1}{2\pi}\oint d\varphi \int_{-\infty}^{+\infty}\frac{d\zeta}{\zeta_0(\xi)}\int_{-\infty}^{+\infty}\frac{d\zeta'}{\zeta_0(\eta)}\frac{\mathrm{sech}^2[\zeta/\zeta_0(\xi)]\mathrm{sech}^2[\zeta'/\zeta_0(\eta)]}{\sqrt{\xi^2+\eta^2-2\xi\eta\cos\varphi+(\zeta-\zeta')^2}}, \tag{F1}$$

where

$$\zeta_0(\xi) = \frac{z_0(\xi)}{\Theta_0^{1/2}a|t|} = \left[\frac{2\left(1-f_0^2\right)}{1+2f_0^2}\right]\frac{1}{\sigma(\xi)}. \tag{F2}$$

It is trivial to show that $\partial\mathcal{H}(0,\eta)/\partial\xi = 0$. Physically, an axisymmetric magnetized disk with finite thickness cannot exert a net radial force at its center if its volume density and current density are regular there.

Although it is possible to develop a multipole expansion procedure for equation (F1), the resulting analysis would be quite involved. For simplicity, therefore, we are content to adopt the alternative treatment of § 5.2 designed to give a physical assessment of the influence of finite disk thickness in the "softened monopole" approximation.

REFERENCES

Adams, F. C., & Fatuzzo, M. 1996, ApJ, 464, 256
Allen, A., Shu, F. H., & Li, Z.-Y. 2003, ApJ, 599, 351
André, P., Ward-Thompson, D., & Barsony, M. 2000, in Protostars and Planets IV, ed. V. Mannings, A. Boss, & S. Russell (Tucson: Univ. Arizona Press), 59
André, P., Ward-Thompson, D., & Motte, F. 1996, A&A, 314, 625
Barenblatt, G. I. 1996, Scaling, Self-Similarity, and Intermediate Asymptotics (Cambridge: Univ. Cambridge Press)
Basu, S., & Mouschovias, T. Ch. 1994, ApJ, 432, 720
Bender, C. M., & Orszag, S. A. 1978, Advanced Mathematical Methods for Scientists and Engineers (New York: McGraw-Hill)

Camm, G. L. 1950, MNRAS, 110, 305
Cassen, P., & Moosman, A. 1981, Icarus, 48, 353
Choi, M., Evans, N. J., Gregersen, E. M., & Wang, Y. 1995, ApJ, 448, 742
Desch, S. J., & Mouschovias, T. Ch. 2001, ApJ, 550, 314
Evans, N. J., Lee, J.-E., Rawlings, J. M. C., & Choi, M. 2005, ApJ, 626, 919
Fatuzzo, M., & Adams, F. C. 2002, ApJ, 570, 210
Fatuzzo, M., Adams, F. C., & Melia, F. 2006, ApJ, 653, L49
Fatuzzo, M., Adams, F. C., & Myers, P. C. 2004, ApJ, 615, 813
Foster, P. N., & Chevalier, R. A. 1993, ApJ, 416, 303
Fromang, S., Hennebelle, P., & Teyssier, R. 2006, A&A, 457, 371
Furuyu, R. S., Kitamura, Y., & Shinnaga, Y. 2006, ApJ, 653, 1369
Galli, D., Lizano, S., Shu, F. H., & Allen, A. 2006, ApJ, 647, 374
Galli, D., & Shu, F. H. 1993, ApJ, 417, 220
Gradshteyn, I. S., & Ryzhik, I. M. 1980, Table of Integrals Series and Products (New York: Academic Press)
Harvey, D. W. A., Wilner, D. J., DiFrancesco, J., Lee, C. W., Myers, P. C., & Williams, J. P. 2002, AJ, 123, 3325
Harvey, D. W. A., Wilner, D. J., Lada, C. J., Myers, P. C., & Alves, J. F. 2003a, ApJ, 598, 1112
Harvey, D. W. A., Wilner, D. J., Lada, C. J., Myers, P. C., Alves, J. F., & Chen, H. 2001, ApJ, 563, 903
Harvey, D. W. A., Wilner, D. J., Myers, P. C., & Tafalla, M. 2003b, ApJ, 596, 383
Heitsch, F., Zweibel, E. G., Slyz, A. D., & Devriendt, J. E. G. 2004, Ap&SS, 292, 45
Henriksen, R. N., André, P., & Bontemps, S. 1997, A&A, 323, 549
Hunter, C. 1977, ApJ, 218, 834
Jackson, J. D. 1962, Classical Electrodynamics (New York: Wiley)
Jijina, J., & Adams, F. C. 1996, ApJ, 462, 874
Jijina, J., Myers, P. C., & Adams, F. C. 1999, ApJS, 125, 161
Krasnopolsky, R., & Königl, A. 2002, ApJ, 580, 987
Lada, C. J., Muensch, A. A., Rathborne, J., Alves, J. F., & Lombardi, M. 2008, ApJ, in press (arXiv: 0709.1164)
Larson, R. B. 1969, MNRAS, 145, 271
Lee, C. W., Myers, P. C., & Tafalla, M. 2001, ApJS, 136, 703
Li, Z. Y., & McKee, C. F. 1996, ApJ, 434, 373
Li, Z.-Y., & Shu, F. H. 1996, ApJ, 472, 211
———. 1997, ApJ, 475, 237
Lizano, S., & Shu, F. H. 1989, ApJ, 342, 834
McKee, C. F. 1989, ApJ, 345, 782
Mestel, L., & Spitzer, L. 1956, MNRAS, 116, 503
Mouschovias, T. Ch. 1976, ApJ, 207, 141
Nakamura, F., & Li, Z.-Y. 2005, ApJ, 631, 411
Nakano, T. 1979, PASJ, 31, 697
———. 1984, Fundam. Cosm. Phys., 9, 139
Ohashi, N., Hayashi, M., Ho, P. T. P., & Momose, M. 1997, ApJ, 475, 211
Penston, M. V. 1969, MNRAS, 144, 425
Price, D. J., & Bate, M. R. 2007, MNRAS, 377, 77
Shu, F. H. 1977, ApJ, 214, 488
———. 1983, ApJ, 273, 202
———. 1992, Gas Dynamics (Mill Valley: Univ. Science)
Shu, F. H., Adams, F. C., & Lizano, S. 1987, ARA&A, 25, 23
Shu, F. H., Galli, D., Lizano, S., & Cai, M. 2006, ApJ, 647, 382
Shu, F. H., Galli, D., Lizano, S., Glassgold, A. G., & Diamond, P. H. 2007, ApJ, 665, 535
Shu, F. H., & Li, Z.-Y. 1997, ApJ, 475, 251
Shu, F. H., Li, Z.-Y., & Allen, A. 2004, ApJ, 601, 930
Shu, F. H., Lizano, S., Galli, D., Cantó, J., & Laughlin, G. 2002, ApJ, 580, 969
Spitzer, L. 1955, Physics of Fully Ionized Gases (New York: Interscience)
Tassis, K., & Mouschovias, T. Ch. 2005, ApJ, 618, 783
Terebey, S., Shu, F. H., & Cassen, P. 1984, ApJ, 286, 529
Walsh, A. J., Myers, P. C., & Burton, M. G. 2004, ApJ, 614, 194
Ward-Thompson, D., Motte, F., & André, P. 1999, MNRAS, 305, 143
Whitworth, A., & Summers, D. 1985, MNRAS, 214, 1
Zhou, S, Evans, N. J., Kömpe, C., & Walmsley, C. M. 1993, ApJ, 404, 232
Zweibel, E. 2002, ApJ, 567, 962